

Acoustic Radiation Impedance of Caps and Rings on Oblate Spheroidal Baffles

R. V. Baier

*Transducer Branch
Acoustics Division*

July 16, 1971



NAVAL RESEARCH LABORATORY
Washington, D.C.

Approved for public release; distribution unlimited



CONTENTS

Abstract	ii
Problem Status	ii
Authorization	ii
INTRODUCTION	1
RADIATION FROM CAPS	2
RADIATION FROM RINGS	7
NUMERICAL COMPUTATION	9
CONCLUSIONS	14
ACKNOWLEDGMENT	14
REFERENCES	40

ABSTRACT

The acoustic radiation impedance seen by curved vibrating caps and rings located on hard baffles of oblate spheroidal shape has been analyzed using eigenfunction expansion in oblate spheroidal wave functions. With the help of extensive computer programs the formulas have been numerically evaluated. The results are presented in families of plotted curves showing the effect of curvature on the acoustic radiation impedance. Calculations were made for ranges in acoustic size of $0.1 \leq ka \leq 20$.

PROBLEM STATUS

This is an interim report on one phase of a continuing NRL Problem.

AUTHORIZATION

NRL Problem S01-29
Project RR 102-08-41-5226

Manuscript submitted September 30, 1970.

ACOUSTIC RADIATION IMPEDANCE OF CAPS AND RINGS ON OBLATE SPHEROIDAL BAFFLES

INTRODUCTION

The radiation of steady-state sound from curved surfaces may be calculated in different ways, depending on the ratio of the effective size of the surface to the wavelength of radiated sound in the medium. For example, when the effective size (the projection of the surface's geodesic diameter onto a plane) is large and the wavelength is small, we may use the methods of geometric acoustics. If however the surface is small and the wavelength large, we may consider the radiation as due to a collection of multipole sources. If the surface is everywhere convex but otherwise characterized by coordinates in which the Helmholtz wave equation is nonseparable, we may calculate the radiation by the Helmholtz integral method, although other methods (such as the creeping wave technique) are equally serviceable. Finally, surfaces which are separable for the Helmholtz wave equation may be calculated by eigenfunction expansions. In the following analyses we shall consider the radiation from an oblate spheroid whose coordinate description forms a separable system for the wave equation. We shall therefore use the convenient method of eigenfunction expansion in a series of oblate spheroidal wave functions.

Let an oblate spheroid be located centrally in a Cartesian system of coordinates (x, y, z) (Fig. 1). The coordinate transformation from Cartesian to oblate spheroidal coordinates (ξ, η, ϕ) is given (1) by

$$\begin{aligned} x &= \frac{d}{2} [(\xi^2 + 1)(1 - \eta^2)]^{1/2} \cos \phi, \\ y &= \frac{d}{2} [(\xi^2 + 1)(1 - \eta^2)]^{1/2} \sin \phi, \\ z &= \frac{d}{2} \xi \eta, \end{aligned} \tag{1}$$

with

$$\begin{aligned} 0 &\leq \xi \leq \infty, \\ -1 &\leq \eta \leq 1, \\ 0 &\leq \phi \leq 2\pi, \end{aligned}$$

where d is the distance between the foci of the spheroid and $\eta = \cos \theta$, in which θ is $1/2$ of the apex angle of the asymptotically tangent cone to $\eta = \eta_0$. The radial parameter $\xi = \text{const.}$ designates a particular oblate spheroid; the polar angle parameter $\eta = \text{const.}$ designates a particular hyperbolic cylinder; the azimuthal angle parameter ϕ when set equal to constant ϕ_0 is a plane through the z axis forming an angle ϕ_0 with the xz plane. The surface $\xi = 0$ is a circular disk of radius $d/2$ which lies in the xy plane and is centered at the origin. The z axis is the axis of rotational symmetry. The degenerate surface $\eta = 1$ is the positive z axis. Considering the intersection of a hyperbolic cylinder with a particular oblate spheroid, we note in Fig. 1 that there results a central annular zone (light shading) and two polar caps (dark shading).

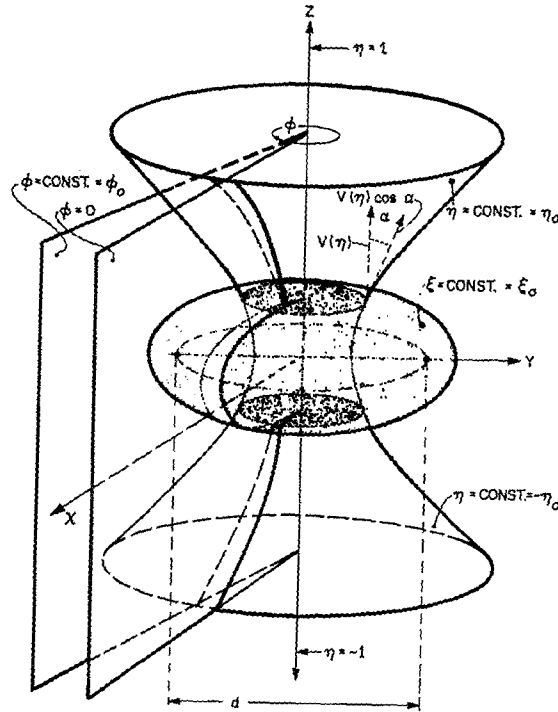


Fig. 1 - Oblate spheroidal coordinate system (ξ, η, ϕ) and the central annular zone (lightly shaded) and polar and caps (dark) on a spheroidal baffle

This report presents computations of the radiation impedance density for caps (pistons) and zones (rings) of various sizes and curvatures on oblate spheroidal baffles of various sizes and eccentricities. Results in the literature to date contained in the work of Bouwkamp (2), Silbiger (3), Chertock (4), Nimura and Watanabe (5) and Hanish (6) are extended in this report to cover wider ranges of piston size, curvature, and frequency.

In Fig. 2 are illustrated some types of vibration of pistons and a ring on an oblate spheroid. The heavily shaded areas are considered to be moving and the lightly shaded as stationary. Figures 2a and 2e illustrate two pistons moving in the direction of the positive z axis, Figs. 2b and 2f illustrate two pistons in opposite motion along the z axis, and Fig. 2c indicate that the field of a single oscillating piston may be obtained by the superposition of the radiation fields of Figs. 2a and 2b. Figures 2d and 2g illustrate a radially vibrating ring on an oblate spheroid.

RADIATION FROM CAPS

The Helmholtz scalar wave equation $(\nabla^2 + k^2) \Phi = 0$ in the velocity potential $\psi = \Phi e^{-i\omega t}$ is separable in oblate spheroidal coordinates. Generally following the notation of Morse and Feshbach (7), we write the eigenfunction series solution (8) for the velocity potential of rings and caps in the form

$$\Phi(\xi, \eta, \phi) = \sum_m \sum_{\ell} B_{m\ell} R_{m\ell}^{(3)}(i\eta, -i\xi) S_{m\ell}(i\eta, \eta) \begin{cases} \cos m\phi \\ \sin m\phi \end{cases},$$

$$\ell = 0, 1, 2, \dots, m = \ell, \ell+1, \ell+2, \dots, \quad (2)$$

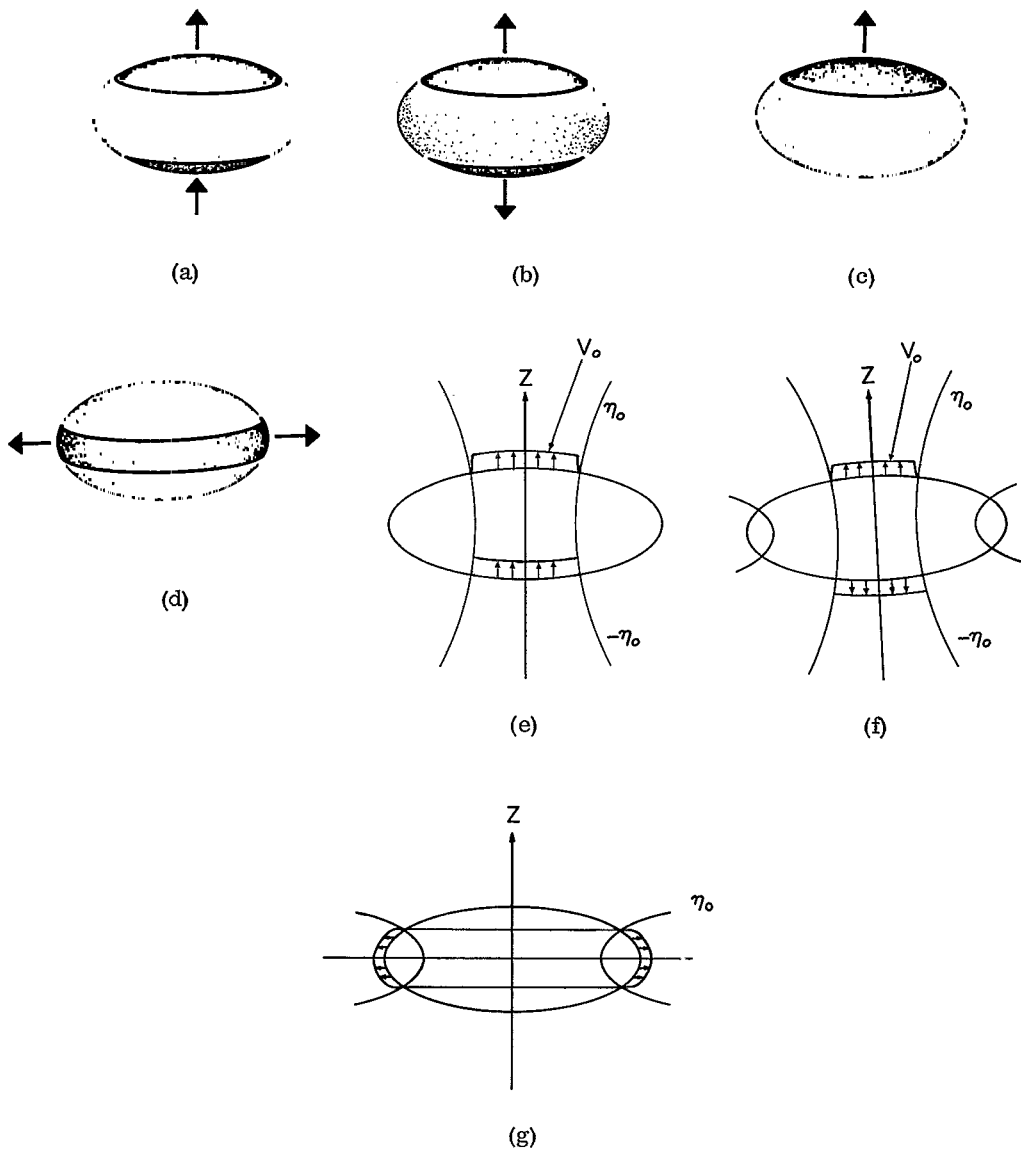


Fig. 2 - Vibrating caps or pistons and a ring on an oblate spheroidal baffle. Figures (e), (f), and (g) are alternate representations of (a), (b), and (d) respectively.

where $\varphi = kd/2$, in which $k = \omega/c$, where ω is the angular frequency and c is the speed of sound in the medium. $R_{m\ell}^{(3)}(i\varphi, -i\xi)$ is an oblate radial wave function of the third kind. $S_{m\ell}(i\varphi, \eta)$ is an oblate angle function of the first kind. The $B_{m\ell}$ are expansion constants (modal amplitudes). The problems considered here are axially symmetric; hence m is zero.

Consider the piston problems illustrated in Figs. 2a and 2e and Figs. 2b and 2f. The pistons are rigid and move parallel to the z axis. At the piston face the particle velocity of the medium in the z direction is given by $\partial\Phi/\partial z = -V(\eta)$ and in the direction of the

normal to the surface is given by $-V(\eta) \cos \alpha$ (Fig. 1). For infinitesimal motion of the rigid curved pistons this particle velocity is equal to the normal (N) component of piston velocity. Thus for the surface $\xi = \xi_0$ we write

$$\left(\frac{\partial \Phi}{\partial N}\right)_{\xi = \xi_0} = -V_0(\eta) (\cos \alpha)_{\xi = \xi_0}.$$

For the case of Figs. 2a and 2e

$$\begin{aligned} V_0(\eta) &= V_0, & \eta_0 \leq \eta \leq 1, \\ &= 0, & -\eta_0 \leq \eta \leq \eta_0, \\ &= -V_0, & -1 \leq \eta \leq -\eta_0, \end{aligned}$$

and for the case of Figs. 2b and 2f

$$\begin{aligned} V_0(\eta) &= V_0, & \eta_0 \leq \eta \leq 1, \\ &= 0, & -\eta_0 \leq \eta \leq \eta_0, \\ &= -V_0, & -1 \leq \eta \leq \eta_0, \end{aligned}$$

where V_0 is the amplitude of the velocity parallel to the z axis and where α is the angle between the z axis and the outward normal to the surface. From the differential geometry of the surface it can be shown that

$$(\cos \alpha)_{\xi = \xi_0} = \left(\frac{\xi^2 + 1}{\xi^2 + \eta^2}\right)_{\xi = \xi_0} \eta.$$

Also,

$$\frac{\partial \Phi}{\partial N} = \frac{1}{h_\xi} \left(\frac{\partial \Phi}{\partial \xi}\right)_{\xi = \xi_0},$$

where $h_\xi(1)$ is the scale factor:

$$h_\xi(1) = \frac{d}{2} \frac{(\xi^2 + \eta^2)^{\frac{3}{2}}}{(1 + \xi^2)^{\frac{3}{2}}}.$$

Performing the indicated operations of Eq. (3) we obtain

$$-\eta \frac{V_0(\eta)}{V_0} \frac{d}{2} V_0 = \sum_{\ell} B_{0\ell} \left[\frac{d}{d\xi} R_{0\ell}^{(3)}(i\eta, -i\xi) \right]_{\xi = \xi_0} S_{0\ell}(i\eta, \eta). \quad (4)$$

Since, by definition, $S_{0\ell}(\eta)$ is orthogonal over the interval $-1 \leq \eta \leq 1$, we multiply both sides of Eq. (4) by S_{0q} and integrate over the interval.

Letting

$$\sigma_{0\ell}(\eta_0) = \int_{-1}^1 \frac{V_0(\eta)}{V_0} S_{0\ell}(\eta) \eta d\eta$$

and

$$N_{0\ell} = \int_{-1}^1 [S_{0\ell}(\eta)]^2 d\eta, \tag{5}$$

we find the expansion coefficients to be

$$B_{0\ell} = \frac{-V_0 \frac{d}{2} \sigma_{0\ell}(\eta_0)}{N_{0\ell} \left[\frac{d}{d\xi} R_{0\ell}^{(3)}(i\eta, -i\xi) \right]_{\xi=\xi_0}}. \tag{6}$$

Substituting Eq. (6) into Eq. (2), the velocity potential becomes

$$\Phi(\xi, \eta) = -\frac{d}{2} V_0 \sum_{\ell} \frac{\sigma_{0\ell}(\eta_0) R_{0\ell}^{(3)}(i\eta, -i\xi) S_{0\ell}(\eta)}{N_{0\ell} \left[\frac{d}{d\xi} R_{0\ell}^{(3)}(i\eta, -i\xi) \right]_{\xi=\xi_0}}. \tag{7}$$

The acoustic pressure is defined by

$$P(\xi, \eta, t) = \rho \frac{\partial \psi}{\partial t} = -ik\rho c \Psi$$

or, omitting time dependence,

$$p(\xi, \eta) = -ik\rho c \Phi,$$

where ρ is the density of the medium. Using Eq. (7), we thus get

$$p(\xi, \eta) = ik \frac{d}{2} \rho c V_0 \sum_{\ell} \frac{\sigma_{0\ell}(\eta_0) R_{0\ell}^{(3)}(i\eta, -i\xi) S_{0\ell}(\eta)}{N_{0\ell} \left[\frac{d}{d\xi} R_{0\ell}^{(3)}(i\eta, -i\xi) \right]_{\xi=\xi_0}}. \tag{8}$$

The mechanical impedance depends on the z component of force F_i of the medium on the area A_i of the piston i , where

$$F_i = \iint_{A_i} p(\xi, \eta) \cos \alpha dA_i,$$

in which

$$\begin{aligned}
 dA_i &= h_\eta d\eta h_\phi d\phi \\
 &= \frac{d}{2} \left(\frac{\xi_0^2 + \eta^2}{1 - \eta^2} \right)^{\frac{1}{2}} d\eta \frac{d}{2} \left[(\xi_0^2 + 1) (1 - \eta^2) \right]^{\frac{1}{2}} d\phi \\
 &= \left(\frac{d}{2} \right)^2 \left[(\xi_0^2 + \eta^2) (1 + \xi_0^2) \right]^{\frac{1}{2}} d\eta d\phi
 \end{aligned} \tag{9}$$

and

$$\cos \alpha dA_i = \left(\frac{d}{2} \right)^2 (1 + \xi_0^2) \eta d\eta d\phi.$$

The symbols h_η and h_ϕ are scale factors as defined in Flammer (1).

Letting

$$\tau_i(\eta_0) = \int_{-1}^1 \epsilon(\eta) S_{0\ell}(\eta) \eta d\eta \tag{10}$$

and $\epsilon(\eta) = 1$ for values of η corresponding to a piston and $\epsilon(\eta) = 0$ for values of η on the baffle (nonmoving surface of the spheroid), then F_i becomes

$$F_i = ik \frac{d}{2} \rho c V_0 2\pi \left(\frac{d}{2} \right)^2 (1 + \xi_0^2) \sum_{\ell} \frac{\sigma_{0\ell}(\eta_0) \tau_i(\eta_0) R_{0\ell}^{(3)}(i\eta, -i\xi_0)}{N_{0\ell} \left[\frac{d}{d\xi} R_{0\ell}^{(3)}(i\eta, -i\xi) \right]_{\xi=\xi_0}} \tag{11}$$

The acoustic radiation impedance Z is given by the ratio of the z component of force F_i to the z component of the surface velocity, i. e., $Z = F_i/V_0$. The complex impedance density \mathcal{Z} is given by

$$\mathcal{Z} = \frac{Z}{\rho c A} = \frac{F_i}{V_0 \rho c A},$$

where A is the total vibrating area. An explicit formula for the impedance density is

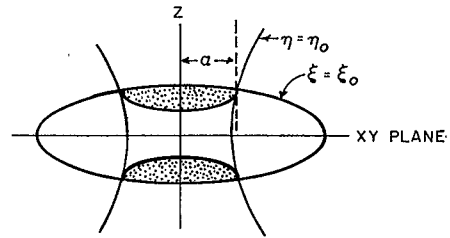
$$\mathcal{Z} = \frac{ikd}{2} \frac{2\pi}{A} \left(\frac{d}{2} \right)^2 (1 + \xi_0^2) \sum_{\ell} \frac{\sigma_{0\ell}(\eta_0) \tau_i(\eta_0) R_{0\ell}^{(3)}(i\eta, -i\xi_0)}{N_{0\ell} \left[\frac{d}{d\xi} R_{0\ell}^{(3)}(i\eta, -i\xi) \right]_{\xi=\xi_0}} \tag{12}$$

Let D be the semimajor axis $\eta = 0$ of the generating ellipse $\xi = \xi_0$; then from Eq. (1). $D = (d/2) (\xi_0^2 + 1)^{\frac{1}{2}}$. Also the radius a of the disk obtained by projecting the cap piston, onto the xy plane (Fig. 3) is

$$a = \frac{d}{2} \left[(\xi_0^2 + 1) (1 - \eta_0^2) \right]^{\frac{1}{2}}.$$

Therefore, $a/D = (1 - \eta_0^2)^{\frac{1}{2}}$. We note that a/D is independent of the parameter ξ , which controls the baffle size.

Fig. 3 - Oscillating caps with radius a



The area A_i of a cap on an oblate spheroid is given by

$$A_i = \pi \left(\frac{d}{2}\right)^2 (1 + \xi_0^2)^{\frac{1}{2}} \left[(1 + \xi_0^2)^{\frac{1}{2}} - \eta_0 (\eta_0^2 + \xi_0^2)^{\frac{1}{2}} + \xi_0^2 \ell n \frac{1 + (1 + \xi_0^2)^{\frac{1}{2}}}{\eta_0 + (\eta_0^2 + \xi_0^2)^{\frac{1}{2}}} \right]. \quad (14)$$

Due to the symmetry in these problems about the xy plane we can set

$$\tau(\eta_0) = 2 \int_{\eta_0}^1 S_{0\ell}(\eta) \eta d\eta = \sigma_{0\ell}(\eta_0). \quad (15)$$

Then the acoustic radiation impedance density may be written as

$$z = i\varphi \frac{2\pi}{A} \left(\frac{d}{2}\right)^2 (1 + \xi_0^2) \sum_{\ell} \frac{\sigma_{0\ell}^2(\eta_0) R_{0\ell}^{(3)}(i\varphi, -i\xi_0)}{N_{0\ell} \left[\frac{d}{d\xi} R_{0\ell}^{(3)}(i\varphi, -i\xi) \right]_{\xi=\xi_0}}. \quad (16)$$

This is the final formula of the analysis of radiation from caps and the one we will use to make numerical computations.

RADIATION FROM RINGS

Consider next a zone (ring) on an oblate spheroidal baffle. Referring to Fig. 1, we describe a zone in functional form as follows:

$$-\eta_0 \leq \eta \leq \eta_0$$

and

$$0 \leq \phi \leq 2\pi.$$

Assume that each point on the ring vibrates with radial velocity $V = V_0$ and the normal velocity is given by

$$V_n = \left(\frac{\partial \Phi}{\partial N} \right)_{\xi=\xi_0} = -V(\eta) (\sin \alpha)_{\xi=\xi_0}. \quad (17)$$

Let $V(\eta) = V_0$ for $-\eta_0 \leq \eta \leq \eta_0$ and let $V(\eta) = 0$ elsewhere as illustrated in Fig. 2g. Performing the operation indicated in Eq. (17), one gets

$$V_0 \frac{d}{2} \left(\frac{1 - \eta^2}{1 + \xi_0^2} \right)^{\frac{1}{2}} \xi_0 \left[\frac{-V(\eta)}{V_0} \right] = \sum_{\ell} B_{0\ell} \left[\frac{d}{d\xi} R_{0\ell}^{(3)}(i\varphi, -i\xi) \right]_{\xi=\xi_0} S_{0\ell}(\eta). \quad (18)$$

Multiplying both sides of Eq. (18) by $S_{0\ell}(\eta)$ and integrating over $-1 \leq \eta \leq 1$, we then obtain (seeing that $S_{0\ell}(\eta)$ is orthogonal over the interval)

$$B_{0\ell} = -\frac{d}{2} \xi_0 V_0 \frac{\int_{-1}^1 \frac{V(\eta)}{V_0} S_{0\ell}(\eta) (1 - \eta^2)^{\frac{1}{2}} d\eta}{N_{0\ell} (1 + \xi_0^2)^{\frac{1}{2}} \left[\frac{d}{d\xi} R_{0\ell}^{(3)}(i\varphi, -i\xi) \right]_{\xi=\xi_0}} \quad (19)$$

Let

$$\mu_{0\ell}(\eta_0) = \int_{-1}^1 \frac{V(\eta)}{V_0} S_{0\ell}(i\varphi, \eta) (1 - \eta^2)^{\frac{1}{2}} d\eta.$$

Then

$$B_{0\ell} = \frac{-\frac{d}{2} \xi_0 \mu_{0\ell}(\eta_0) V_0}{(1 + \xi_0^2)^{\frac{1}{2}} N_{0\ell} \left[\frac{d}{d\xi} R_{0\ell}^{(3)}(i\varphi, -i\xi) \right]_{\xi=\xi_0}}$$

Equation (2) becomes

$$\Phi(\xi, \eta) = \frac{-V_0 \frac{d}{2} \xi_0}{(1 + \xi_0^2)^{\frac{1}{2}}} \sum_{\ell} \frac{\mu_{0\ell}(\eta_0) S_{0\ell}(\eta) R_{0\ell}^{(3)}(i\varphi, -i\xi)}{N_{0\ell} \left[\frac{d}{d\xi} R_{0\ell}^{(3)}(i\varphi, -i\xi) \right]_{\xi=\xi_0}} \quad (20)$$

and the acoustic pressure becomes

$$\begin{aligned} p(\xi, \eta) &= -ik\rho c\Phi \\ &= \frac{i\rho c V_0 \varphi \xi_0}{(1 + \xi_0^2)^{\frac{1}{2}}} \sum_{\ell} \frac{\mu_{0\ell}(\eta_0) R_{0\ell}^{(3)}(i\varphi, -i\xi) S_{0\ell}(\eta)}{N_{0\ell} \left[\frac{d}{d\xi} R_{0\ell}^{(3)}(i\varphi, -i\xi) \right]_{\xi=\xi_0}}, \end{aligned} \quad (21)$$

where $\varphi = kd/2$. The projection of the medium reaction force F onto the xy plane is

$$F = \iint_A p(\xi, \eta) \sin \alpha \, dA.$$

Substituting known relations for p , $\sin \alpha$, and dA into this integral, then

$$F = i q \rho c V_0 2\pi \left(\frac{d}{2}\right)^2 \sum_{\ell}^{\xi_0^2} \frac{\mu_{0\ell}(\eta_0) R_{0\ell}^{(3)}(iq, -i\xi) \int_{-1}^1 S_{0\ell}(\eta) (1-\eta^2)^{\frac{1}{2}} d\eta}{N_{0\ell} \left[\frac{d}{d\xi} R_{0\ell}^{(3)}(iq, -i\xi) \right]_{\xi=\xi_0}} \quad (22)$$

Since $V(\eta)/V_0 = 1$ over the ring, then

$$\mu_{0\ell}(\eta_0) = \int_{-1}^1 S_{0\ell}(iq, \eta) (1-\eta^2)^{\frac{1}{2}} d\eta.$$

Equation (22) allows us to formulate the radiation mechanical impedance density \mathfrak{z} of a ring, where $\mathfrak{z} = F/V \rho c A$, in which A is the surface area of the ring, as follows:

$$\mathfrak{z} = \frac{i q 2\pi \left(\frac{d}{2}\right)^2}{A} \sum_{\ell}^{\xi_0^2} \frac{\mu_{0\ell}^2(\eta_0) R_{0\ell}^{(3)}(iq, -i\xi_0)}{N_{0\ell} \left[\frac{d}{d\xi} R_{0\ell}^{(3)}(iq, -i\xi) \right]_{\xi=\xi_0}} \quad (23)$$

The area A of a ring on an oblate spheroid is

$$A = 2\pi \left(\frac{d}{2}\right)^2 (1 + \xi_0^2)^{\frac{1}{2}} \left[\eta_0 (\xi_0^2 + \eta_0^2)^{\frac{1}{2}} + \xi_0^2 \ln \frac{\eta_0 + (\xi_0^2 + \eta_0^2)^{\frac{1}{2}}}{\xi_0} \right] \quad (24)$$

Equation (23) is the final equation of the analysis. We will use it for making numerical computations. We have plotted numerical values in terms of q with η_0 as a parameter. Below are listed some relationships relating ring dimensions to the spheroidal coordinates parameters, where $2D$ is the maximum diameter of the ring and b is the axial height of the ring:

$$b = 2z = d\xi\eta \quad \text{and} \quad D = \frac{d}{2} (1 + \xi^2)^{\frac{1}{2}},$$

so that

$$\frac{b}{D} = \frac{2\xi\eta}{(1 + \xi^2)^{\frac{1}{2}}}.$$

NUMERICAL COMPUTATION

The mechanical radiation impedance of moving caps on oblate spheroidal baffles has been calculated by the use of Eq. (16). In the first instance the caps are made to have zero curvature; i. e., they are flat circular disks in flat circular baffles. The important parameters are the ratio a/D of disk radius to baffle radius and the acoustic size $ka = 2\pi a/\lambda$ of the disk. This case has been treated by Nimura and Watanabe (5) for smaller ranges of the parameters. We have calculated the radiation mechanical impedance density (see Eq. (16)) and have plotted \mathfrak{z} vs ka for various values of a/D . Our results are shown in Fig. 4, where we have plotted the resistance density \mathfrak{z}_R for the following special cases: infinite baffle (D infinite and a finite), no baffle ($D = a$), and $a/D = 0.1736, 0.342, 0.5000, 0.6499, \text{ and } 0.8660$. Figures 4, 5a and 5b show the same case as Fig. 4 except that we have plotted the reactance impedance density \mathfrak{z}_I in lieu of \mathfrak{z}_R . Figures 4 and 5 stand as models of the type of calculation to be found in the figures to follow for

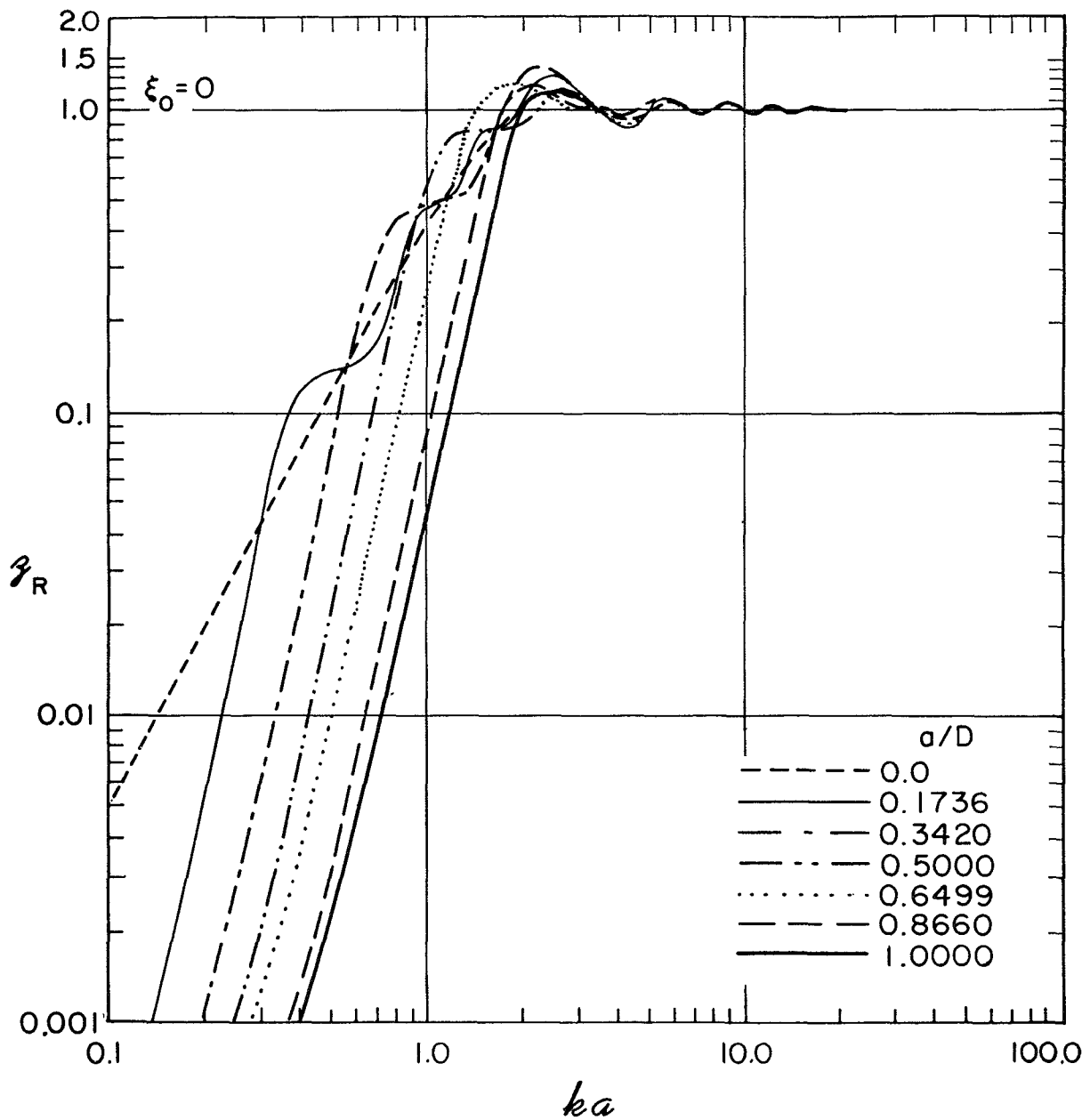


Fig. 4 - Radiation resistance density for a flat circular disk as a function of ka for several values of the ratio of the piston size to the baffle size (for l odd, except $a/D = 0$)

caps on oblate spheroids, with the addition that the later series of figures (6 through 20) illustrate the effect of changing the curvature of the radiating surface. Figures 21 through 25 present the mechanical radiation impedance, Eq. (23), for zones of rings on oblate spheroidal baffles as a function of $q = kd/2$ with η as a parameter. We list these figures in Tables 1 and 2, together with pertinent remarks. It is to be noted that the oscillating caps and rings used in these figures are defined by the intersection of the hyperboloid $|\eta| = \eta_0$ of two sheets with the spheroid $\xi = \xi_0$, having the same axis of revolution. The radius a is the projection of the radius of the curved cap onto the xy plane (Fig. 3).

Table 1
Summary of Figures for Caps, Which are Plots of the Radiation Impedance Density (Radiation Resistance Density \mathcal{Z}_R and Reactance Density \mathcal{Z}_I) vs ka of Two Oscillating Caps that Extend to $\eta = \eta_0$ on an Oblate Spheroid with Some or All of the Parameters $\xi = 0, 0.2, 0.4, 0.6, 0.9,$ and 2.0

Fig. No.	Motion of the Two Caps	Value of η_0	Fig. No.	Motion of the Two Caps	Value of η_0
6	Opposite directions	0	13	Opposite directions	0.76
7	Same direction	0	14	Same direction	0.76
8	Comparison of \mathcal{Z}_R and \mathcal{Z}_I vs ka for an oscillating disk in an infinite baffle and a disk with no baffle		15	Opposite directions	$\sqrt{3}/2$
			16	Same direction	$\sqrt{3}/2$
9	Opposite directions	0.5	17	Opposite directions	0.9397
10	Same direction	0.5	18	Same direction	0.9397
11	Opposite directions	0.6	19	Opposite directions	0.9848
12	Same direction	0.6	20	Same direction	0.9848

Table 2
Summary of Figures for Disks, Which are Plots of the Radiation Resistance Density \mathcal{Z}_R and Reactance Density \mathcal{Z}_I vs $q (= kd/2)$ of Rings on an Oblate Spheroid Defined by $\eta_0 = 0.1736, 0.2558, 0.5000, 0.7071, 0.8660,$ and 1.000

Fig. No.	ξ_0	Impedance
21a	0.6	\mathcal{Z}_R
21b	0.6	\mathcal{Z}_I
22a	0.75	\mathcal{Z}_R
22b	0.75	\mathcal{Z}_I
23a	0.90	\mathcal{Z}_R
23b	0.90	\mathcal{Z}_I
24a	1.0	\mathcal{Z}_R
24b	1.0	\mathcal{Z}_I
25a	2.0	\mathcal{Z}_R
25b	2.0	\mathcal{Z}_I

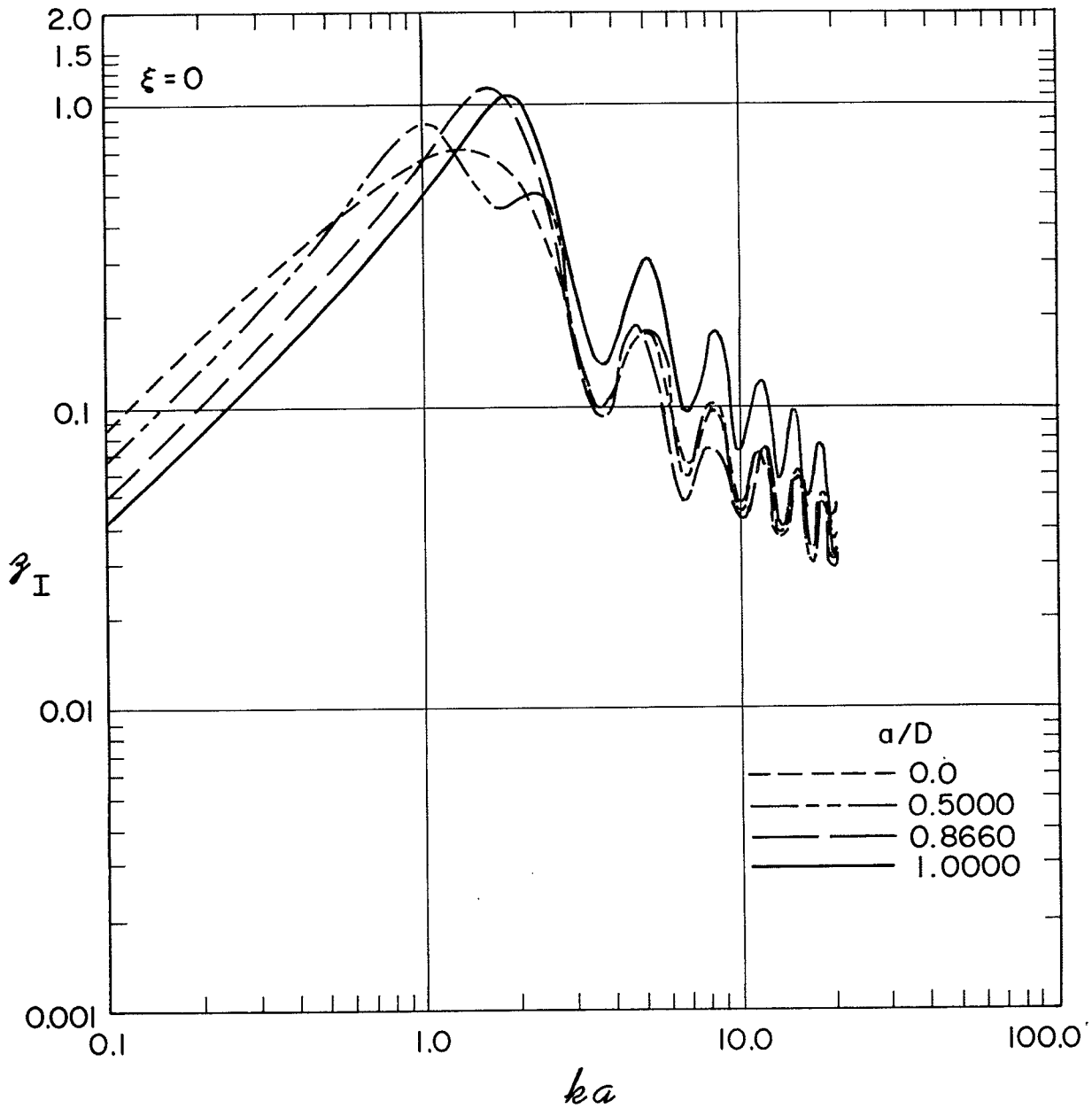


Fig. 5a - Radiation reactance density for a flat circular disk as a function of ka for several values of the ratio of the piston size to the baffle size (for ℓ odd, except $a/D = 0$). (Additional curves are given in Fig. 5b.)

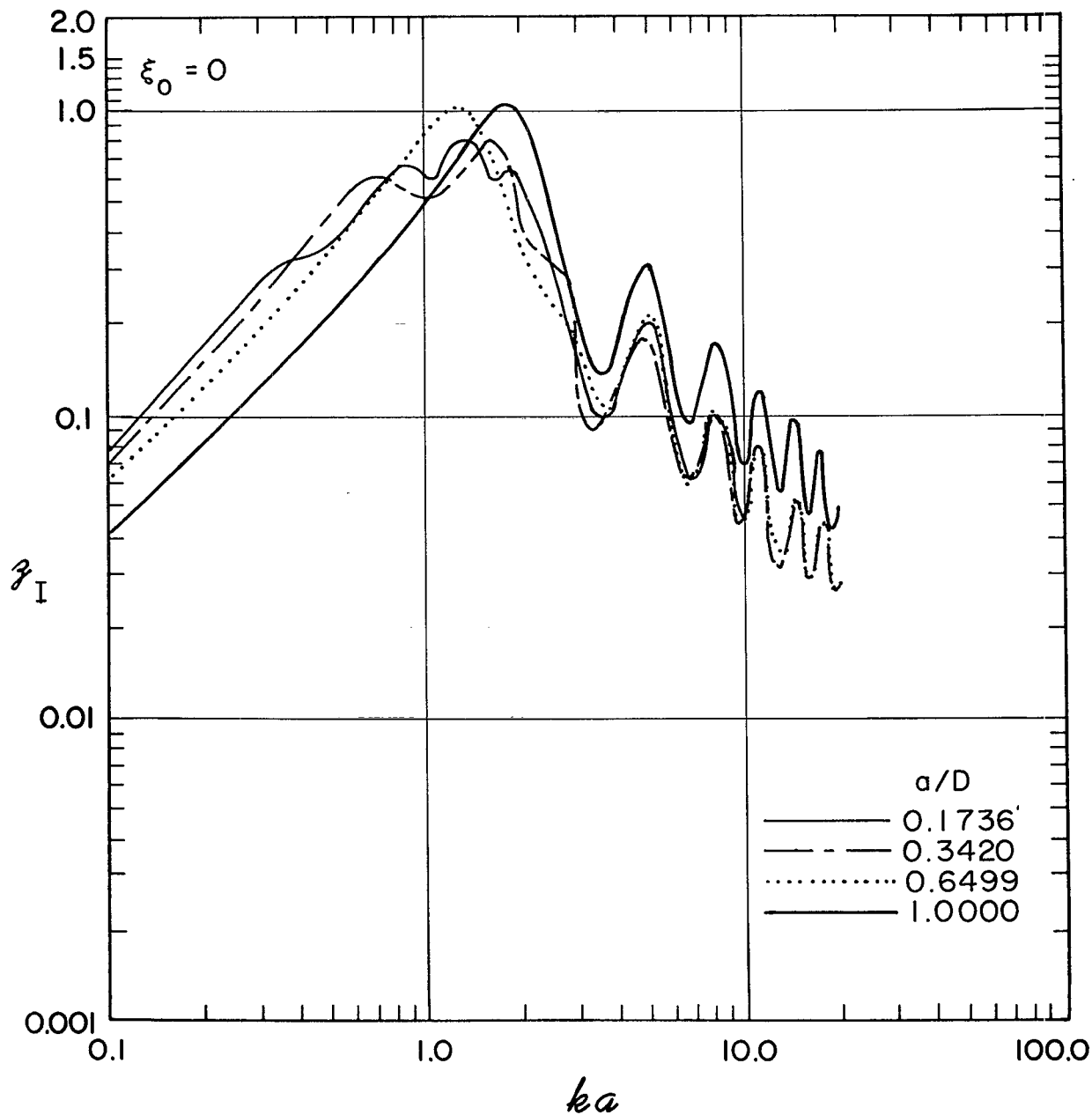


Fig. 5b - Additional curves for Fig. 5a

In those formulas derived above where the spheroidal wave functions $R_{0\ell}^{(3)}$, $dR_{0\ell}^{(3)}/d\xi$, and $S_{0\ell}$ occur, their numerical computation is effected by use of the NRL-developed computer programs called OBRAD (9) and ANGLFN (10). Without these programs the calculations of radiation impedance over the extended ranges displayed in the following families of figures would have been extremely difficult.

CONCLUSIONS

The effect of baffle curvature on radiation impedance has been illustrated by families of curves involving thousands of computed points. Figures 4 and 5 demonstrate that the radiation impedance density is strongly dependent on the baffle size for flat circular disks ($ka \leq 1$) and is largely independent of the baffle size when $ka \geq 2$. Figures 6 through 20, showing piston radiation impedances, indicate that for large ka the oscillating (odd ℓ) and the pulsating (even ℓ) spheroids with the same eccentricity and baffle have nearly the same impedance density; in fact asymptotically (that is, $\xi \rightarrow \infty$) they approach the same limit.

Figures 21 through 25 illustrate that for large values of the parameter q the radiation resistance density diminishes as τ_0 varies from zero to unity (as the axial height of the rings varies from small to large). The reason for this behavior can be understood by considering the curved nature of the radiating surface and the definition of impedance density. The impedance density as defined here is the ratio of the medium reaction force projected onto the xy plane (Fig. 1) to the product of velocity V_0 (constant) of the ring and the total vibrating area of the ring. Since the projected reaction force diminishes as the ring height increases, and since further the ring area increases as the ring height increases, it is seen that the ratio diminishes. The diminution of the reaction force as the ring height increases is due to the ring surface becoming more curved as the ring encompasses more of the total spheroid. For small q (wavelength large compared to vibrating ring) the reaction force is essentially independent of the geometry; hence the impedance density simply follows the radiation impedance density of simple sources.

Not presented here, but now well within our computation capability, is the computation of near-field and far-field pressure patterns which involve the use of angle spheroidal wave functions. An effective Fortran IV subroutine for obtaining these functions is also available (9).

ACKNOWLEDGMENT

I gratefully acknowledge the important contributions of Marvin Blizzard for the computer programming and obtaining part of the data used in this report.

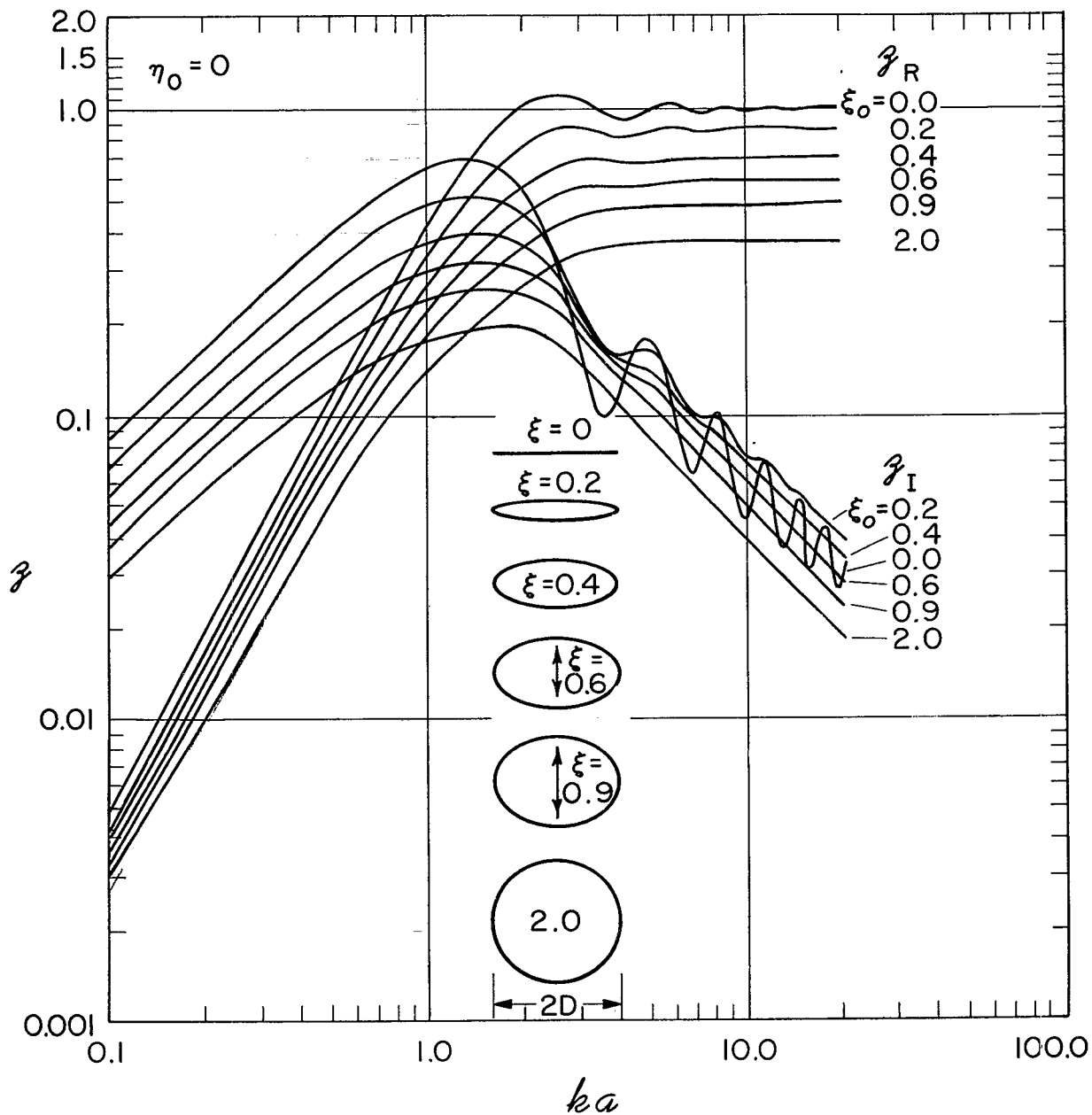


Fig. 6 - Radiation impedance density (resistance density z_R and reactance density z_I) as a function of ka , where a is the radius of the resulting disk obtained by projecting the piston ($\eta_0 = 0$) onto the xy plane for a series of rigid oblate spheroids vibrating along the z axis (even values of ℓ)

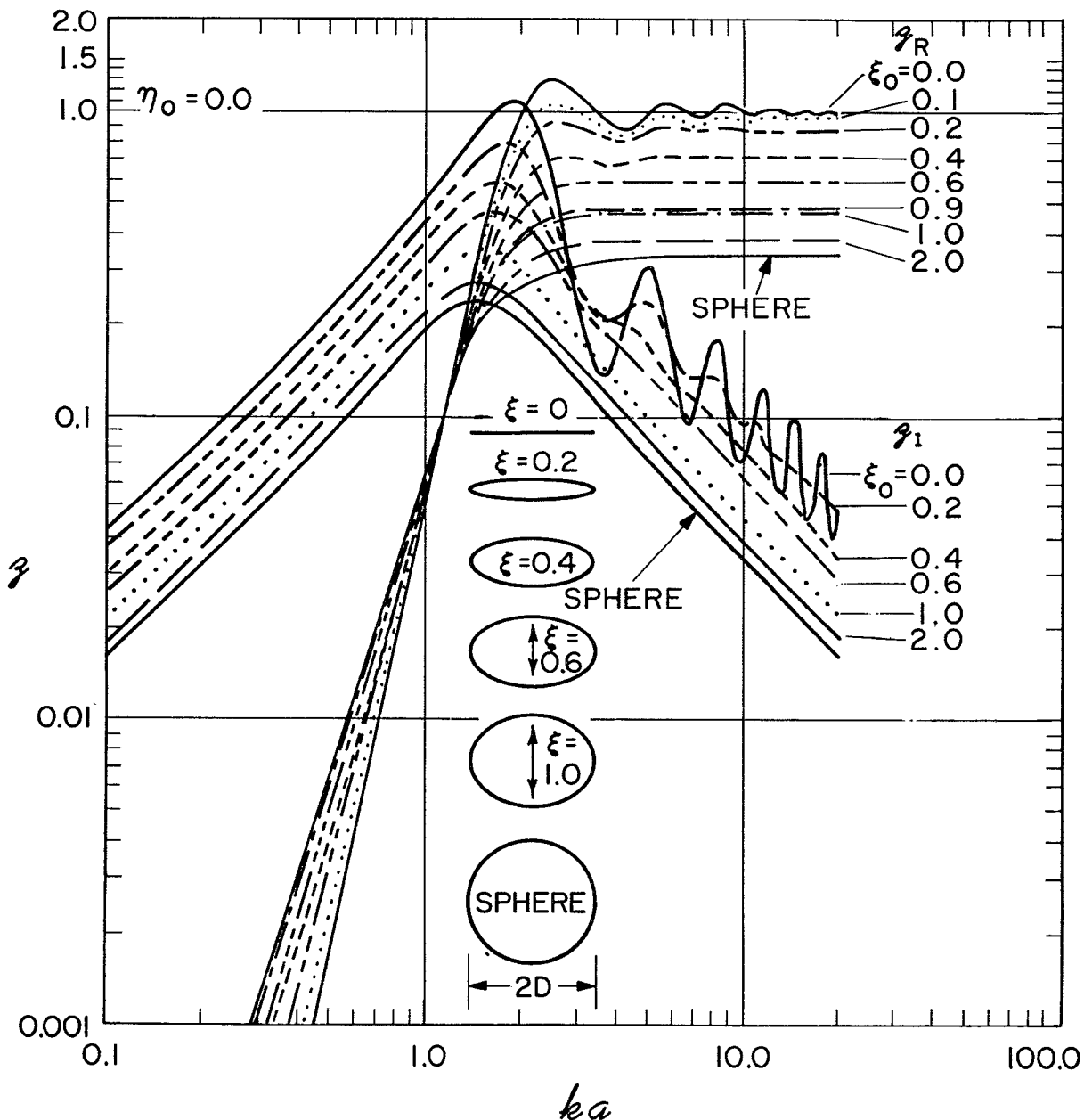


Fig. 7 - Radiation impedance density as a function of ka , where a is the radius of the disk obtained by projecting the piston ($\eta_0 = 0$) onto the xy plane for a series of rigid oblate spheroids vibrating along the z axis (odd values of ℓ)

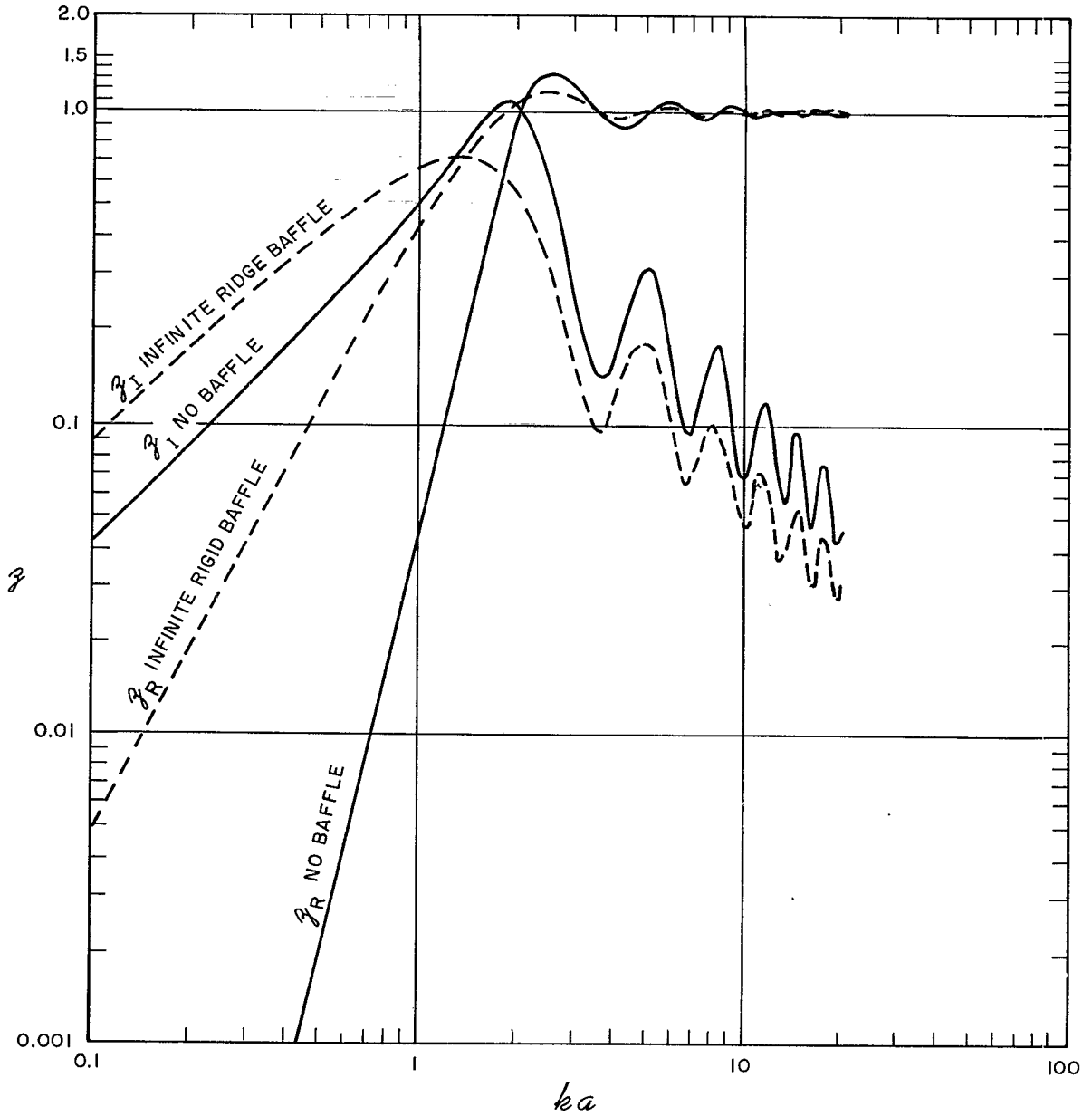


Fig. 8 - Radiation impedance density for a rigid circular disk without a baffle and in a rigid infinite plane baffle as a function of ka

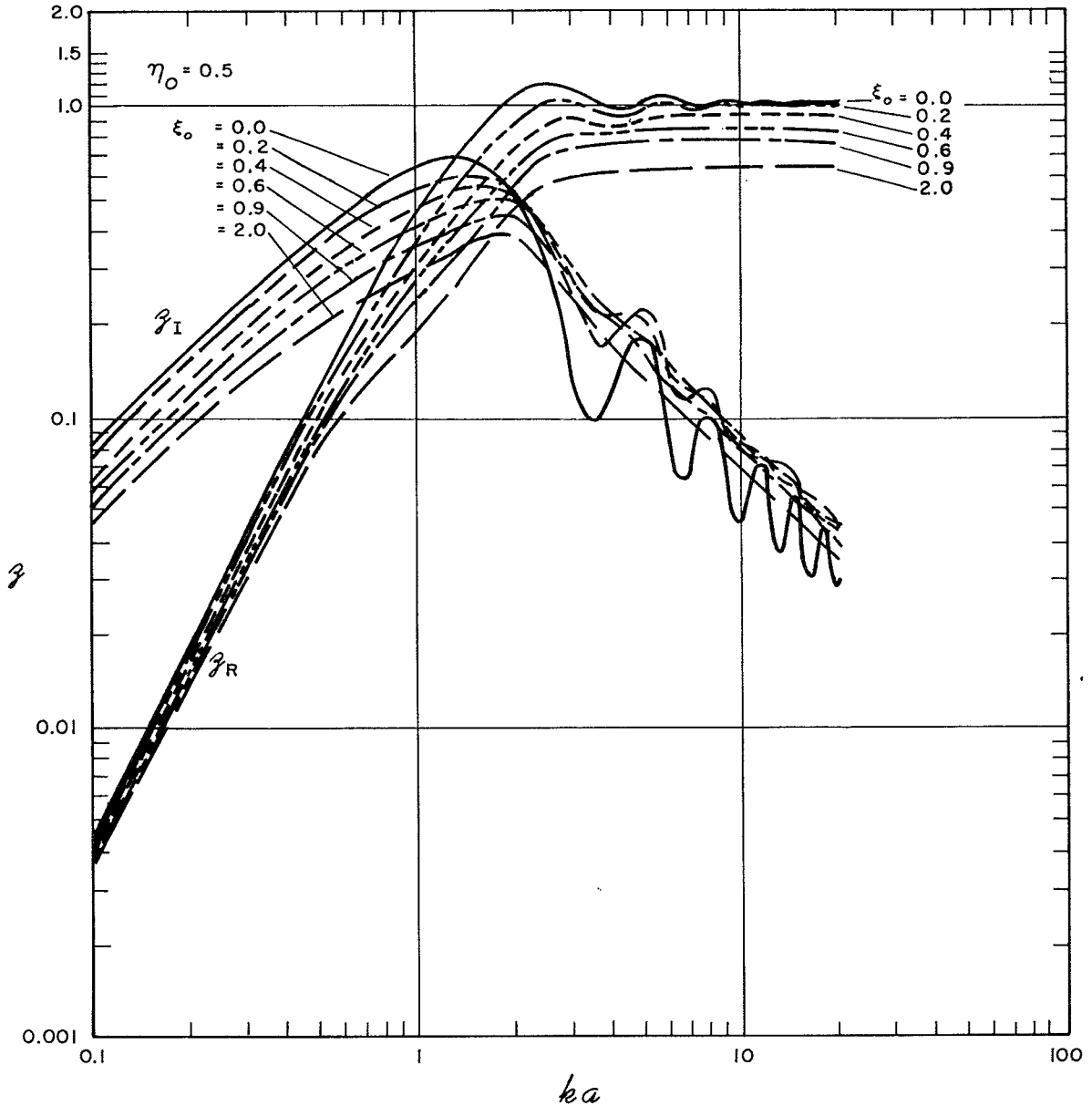


Fig. 9 - Radiation impedance density as a function of ka , where a is the radius of the resulting disk obtained by projecting the piston ($\eta_0 = 0.5$) onto the xy plane for even values of ℓ

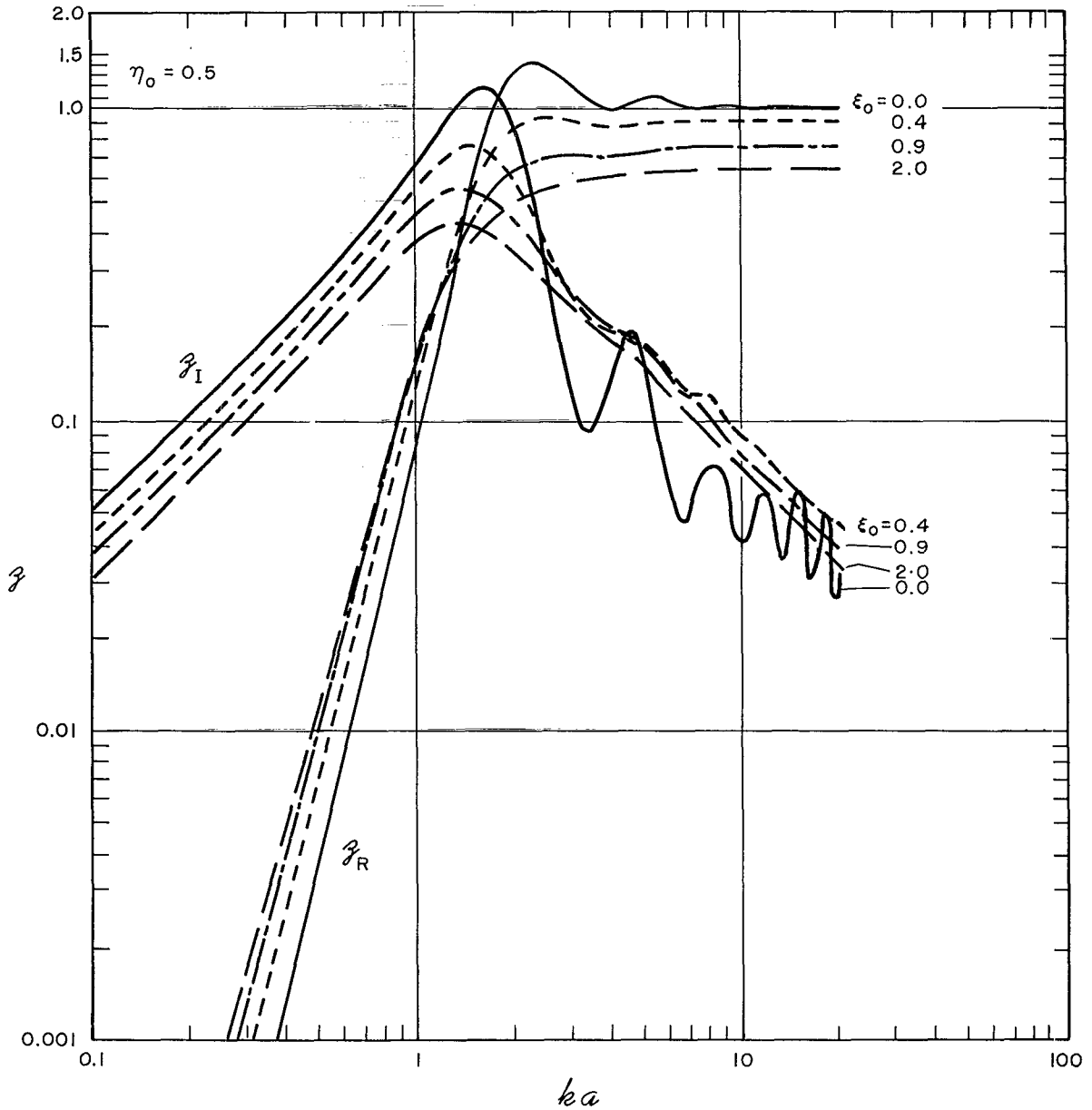


Fig. 10 - Radiation impedance density as a function of ka , where a is the radius of the resulting disk obtained by projecting the piston ($\eta_0 = 0.5$) onto the xy plane for odd values of ℓ

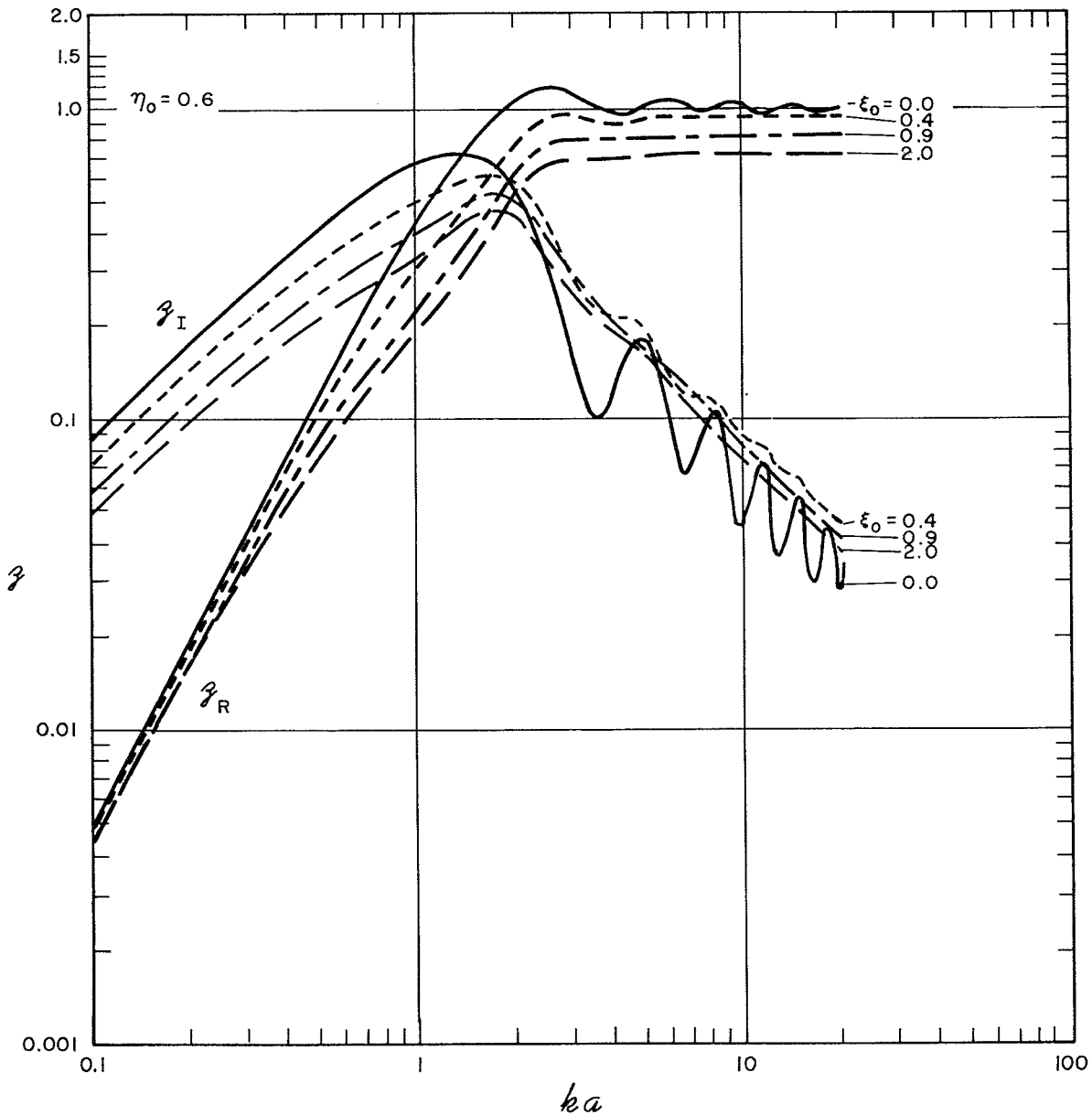


Fig. 11 - Radiation impedance density as a function of ka , where a is the radius of the resulting disk obtained by projecting the piston ($\eta_0 = 0.6$) onto the xy plane for even values of ℓ

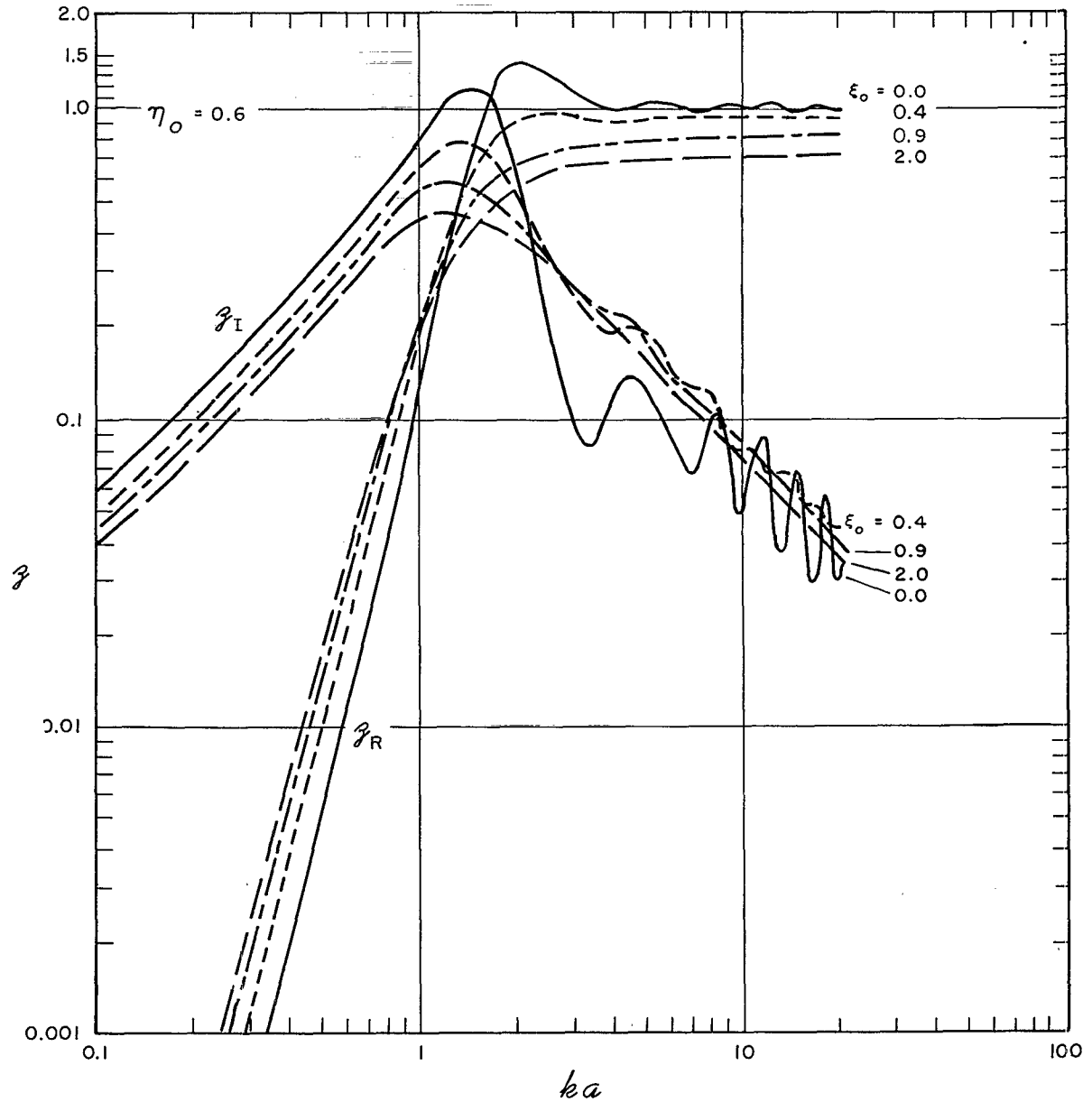


Fig. 12 - Radiation impedance density as a function of ka , where a is the radius of the resulting disk obtained by projecting the piston ($\eta_0 = 0.6$) onto the xy plane except for odd values of ℓ

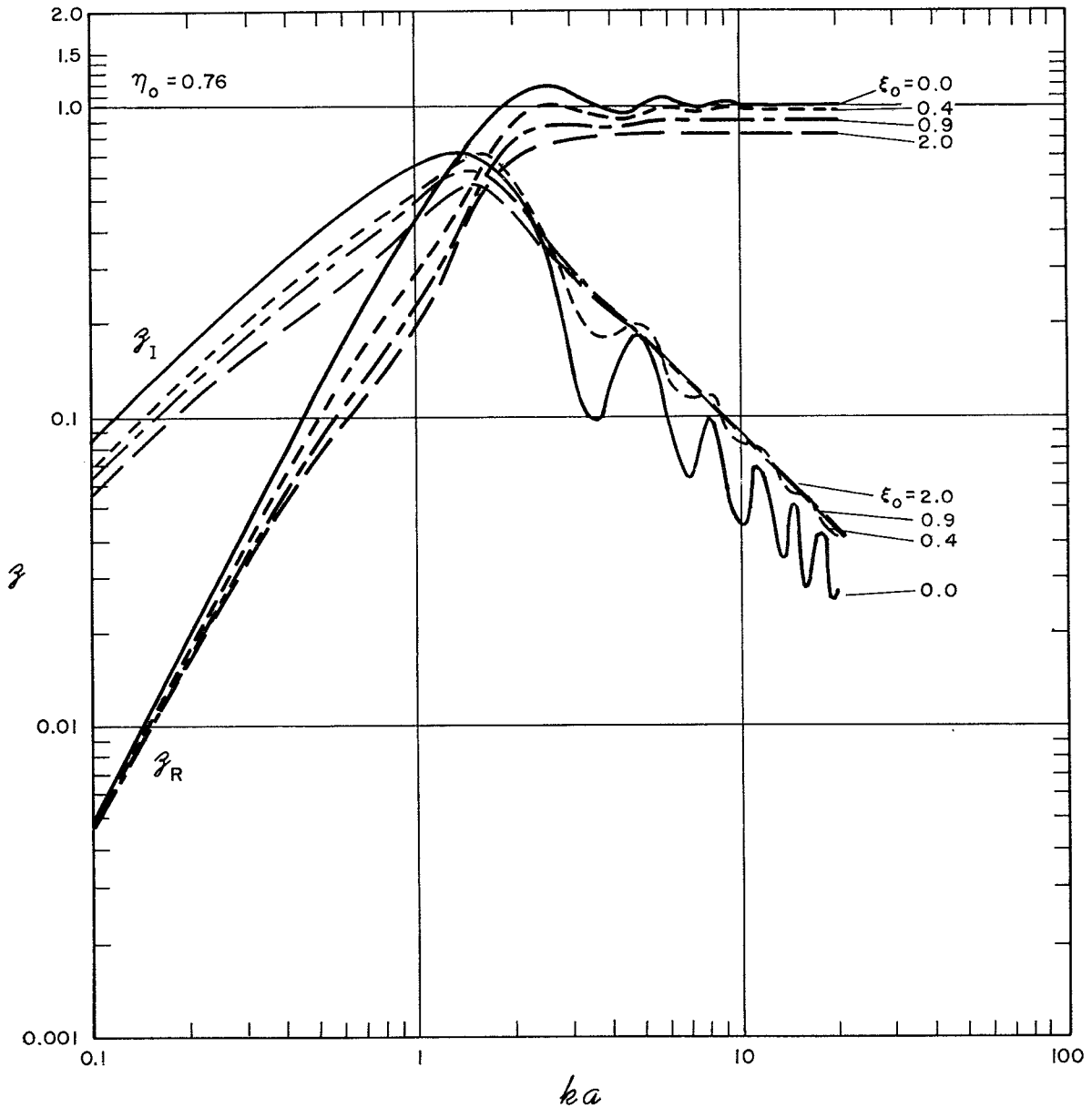


Fig. 13 - Radiation impedance density as a function of ka where a is the radius of the resulting disk obtained by projecting the piston ($\eta_0 = 0.76$) onto the xy plane for even values of ℓ

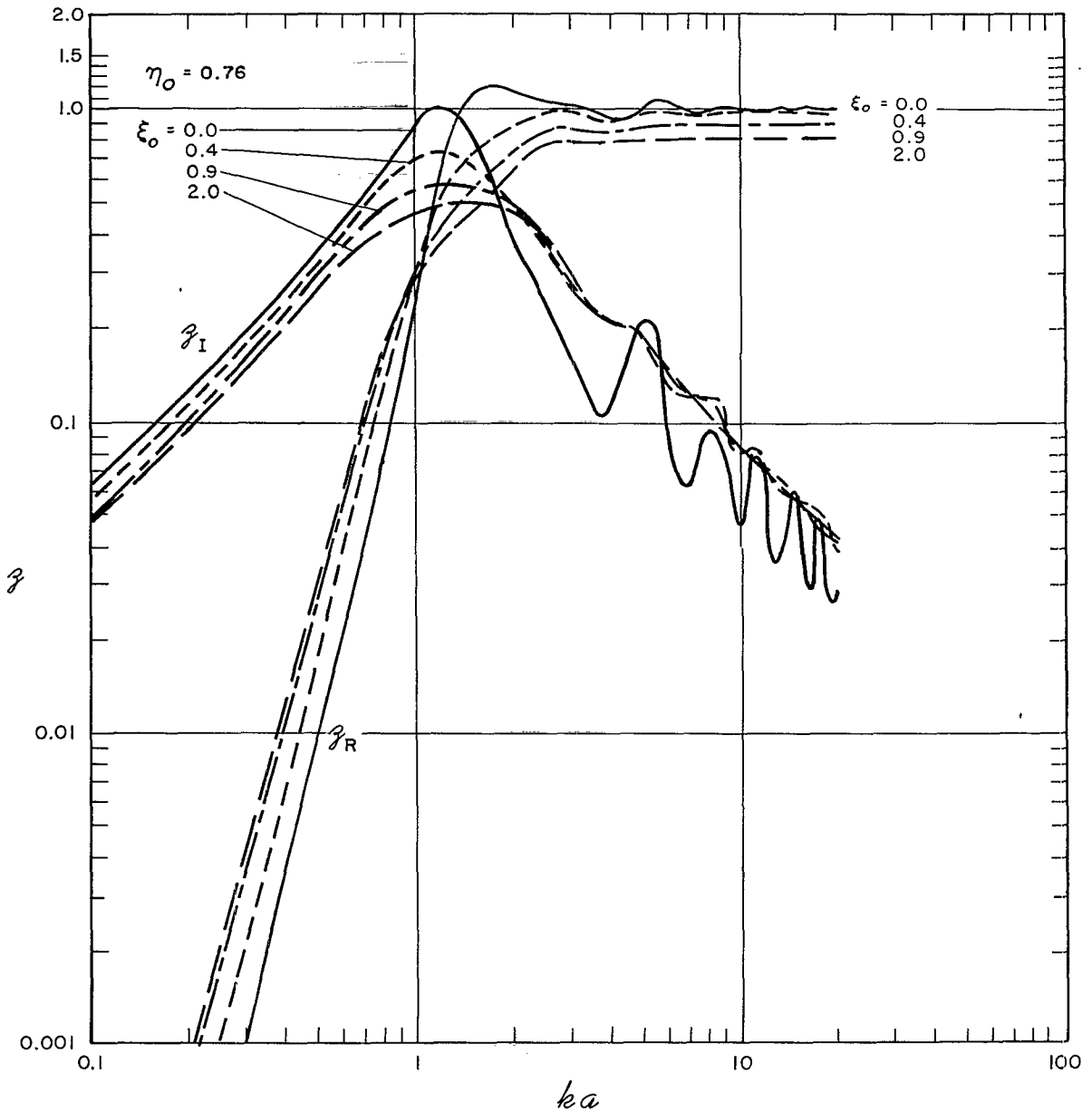


Fig. 14 - Radiation impedance density as a function of ka when a is the radius of the resulting disk obtained by projecting the piston ($\eta_0 = 0.76$) onto the xy plane for odd values of ℓ

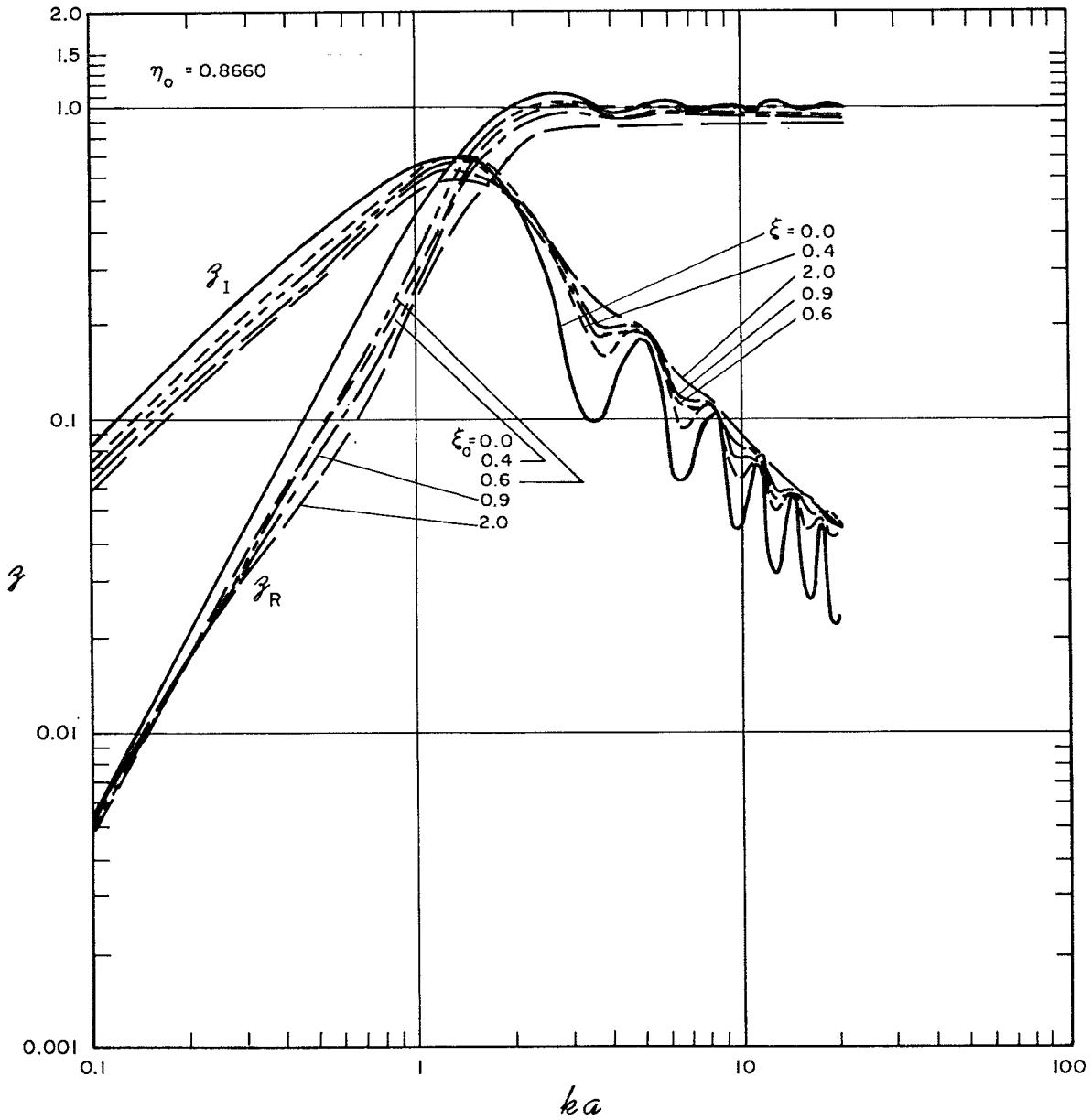


Fig. 15 - Radiation impedance density as a function of ka , where a is the radius of the resulting disk obtained by projecting the piston ($\eta_0 = \sqrt{3}/2$) onto the xy plane for even values of ℓ

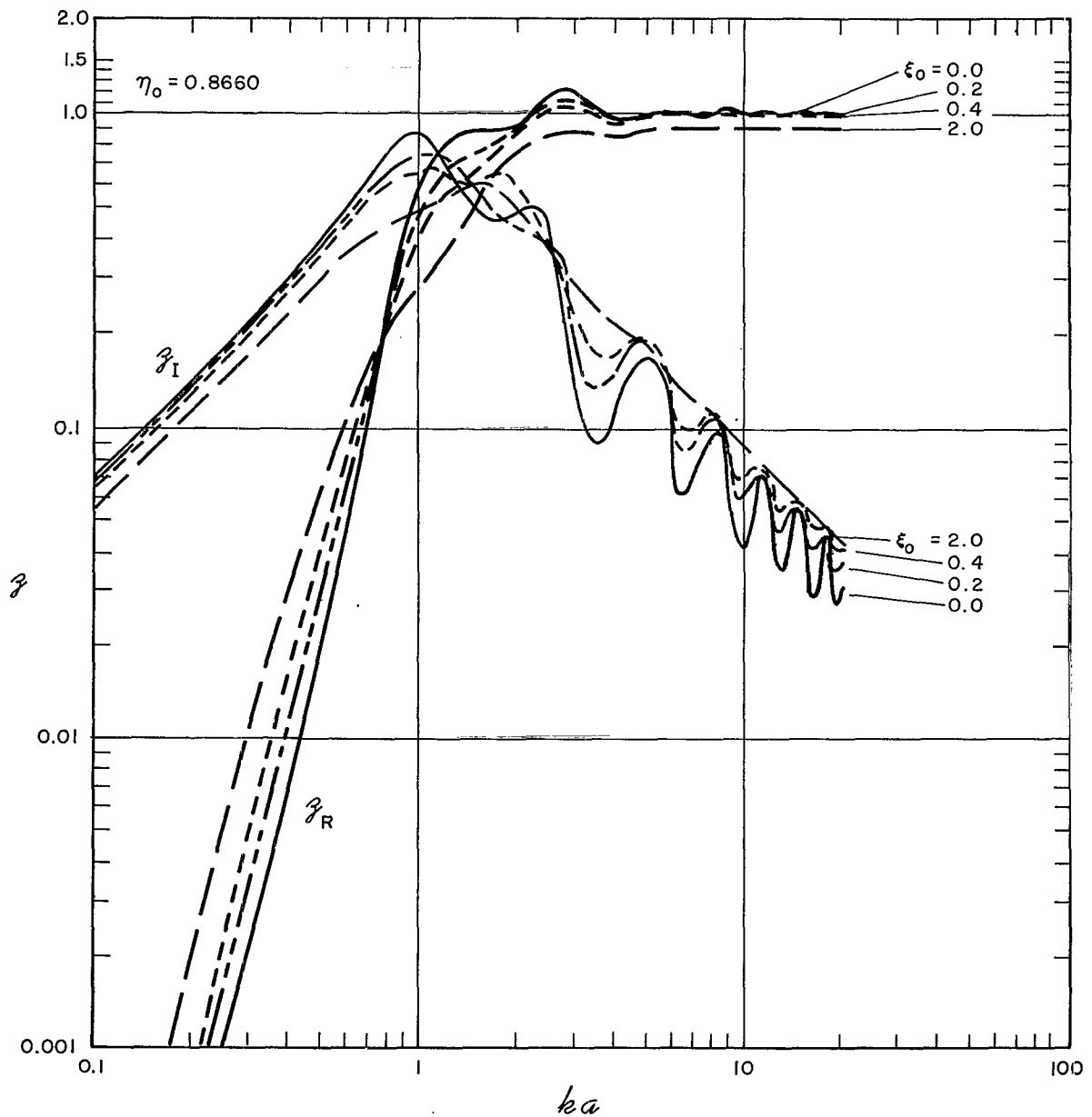


Fig. 16 - Radiation impedance density as a function of ka , where a is the radius of the resulting disk obtained by projecting the piston ($\eta_0 = \sqrt{3/2}$) onto the xy plane for odd values of ℓ

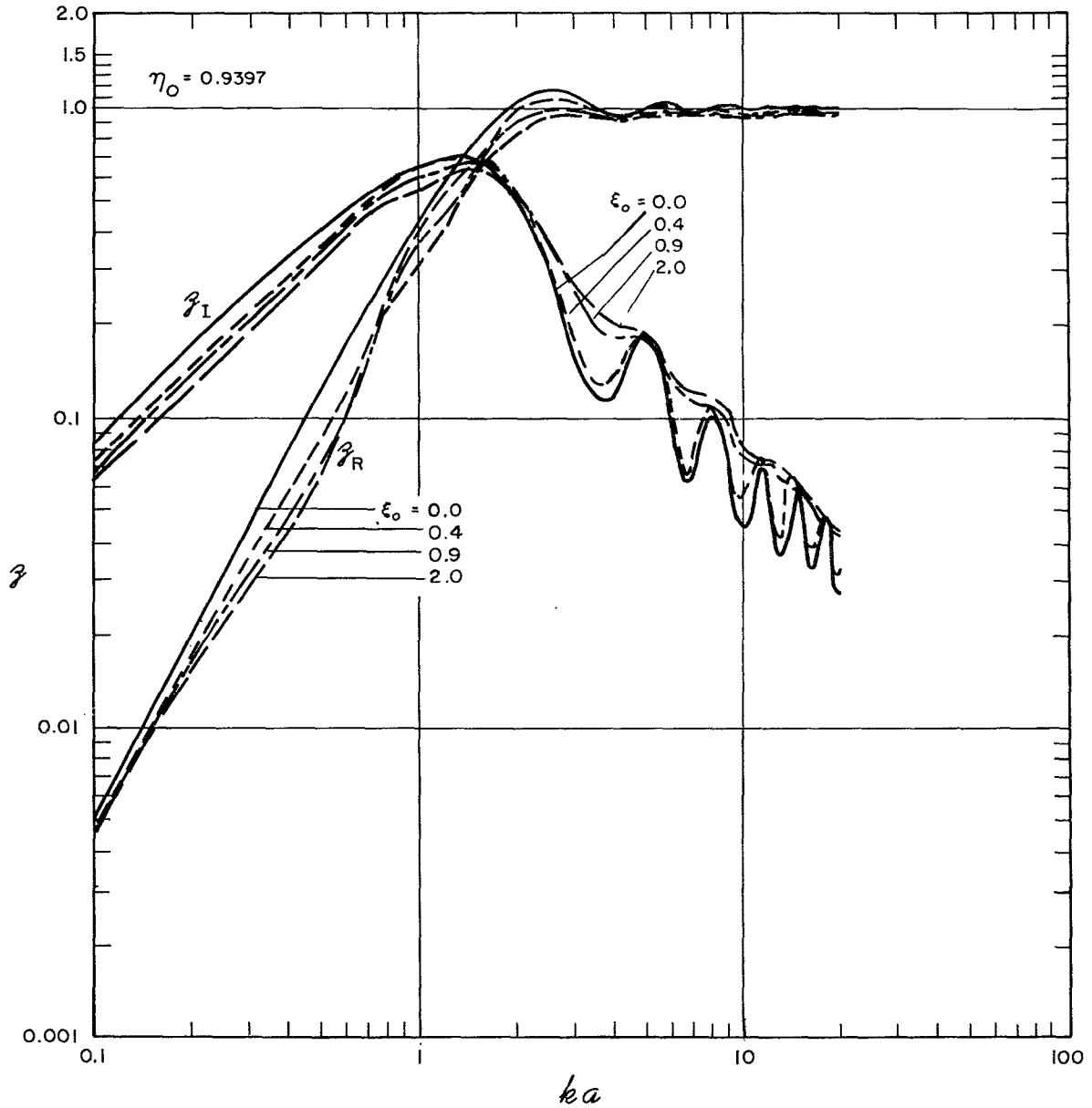


Fig. 17 - Radiation impedance density as a function of ka , where a is the radius of the resulting disk obtained by projecting the piston ($\eta_0 = 0.9397$) onto the xy plane for even values of ℓ

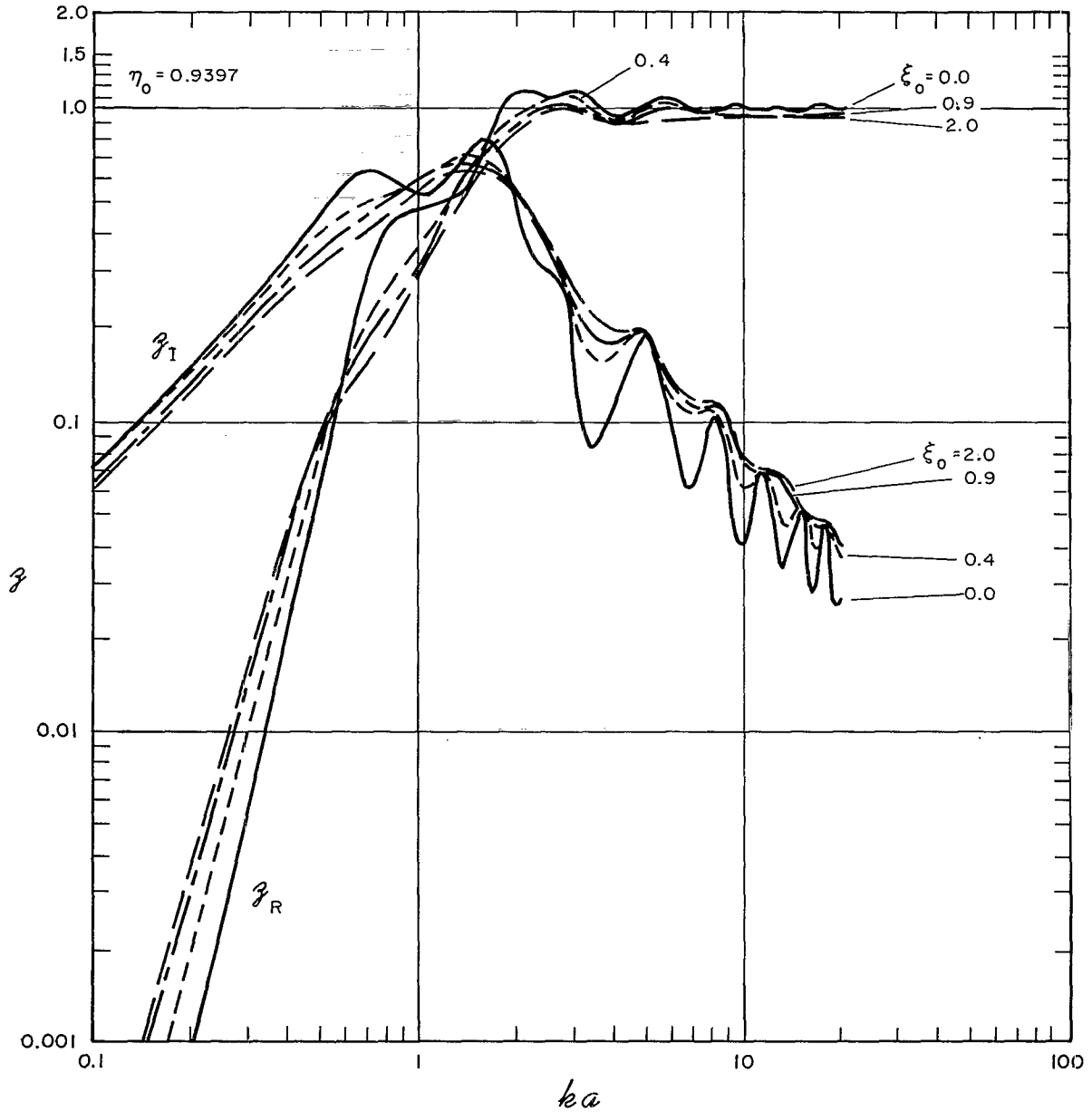


Fig. 18 - Radiation impedance density as a function of ka , where a is the radius of the resulting disk obtained by projecting the piston ($\eta_0 = 0.9397$) onto the xy plane for odd values of ℓ

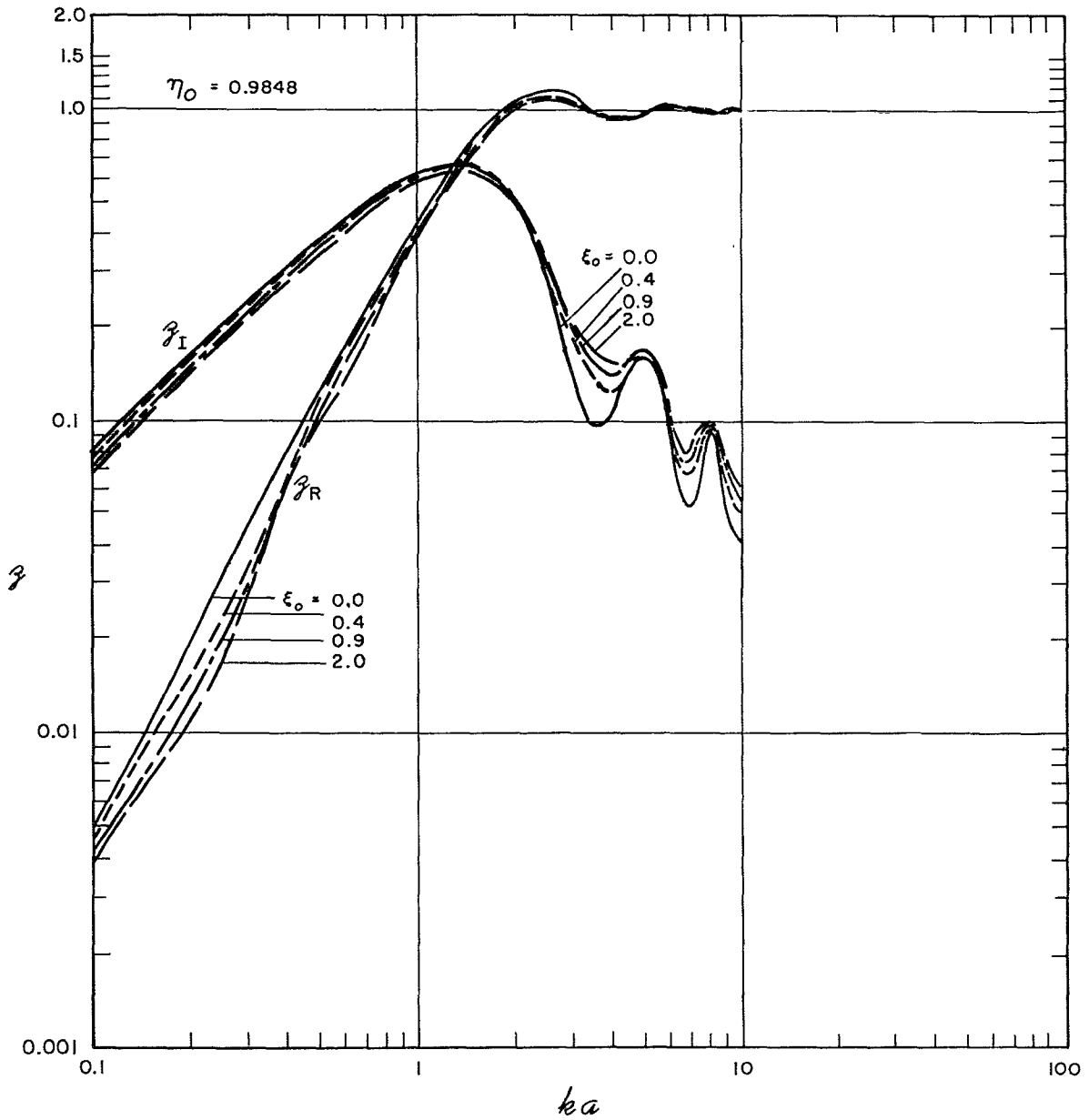


Fig. 19 - Radiation impedance density as a function of ka , where a is the radius of the resulting disk obtained by projecting the piston ($\eta_0 = 0.9848$) onto the xy plane for even values of ℓ

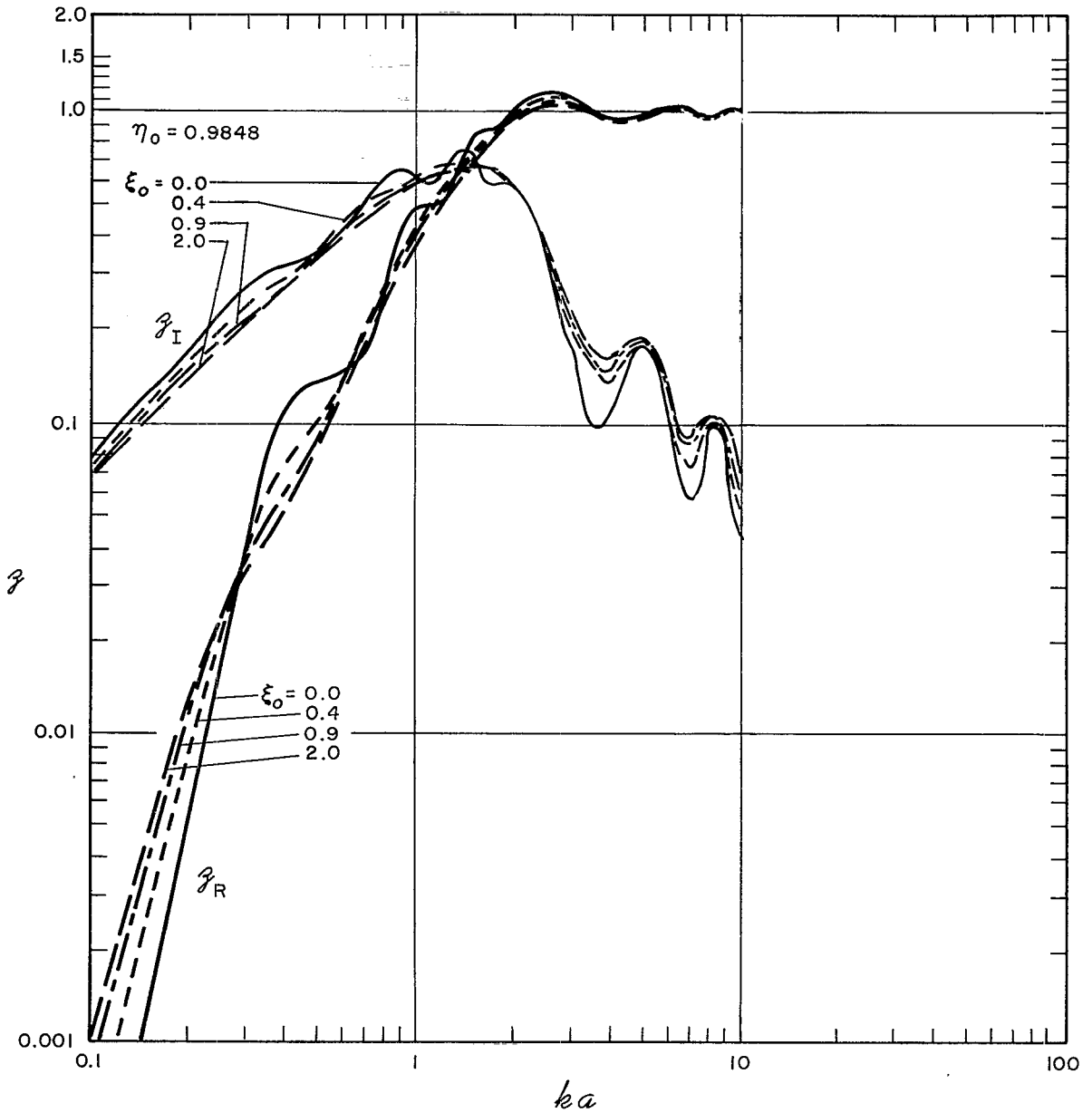


Fig. 20 - Radiation impedance density as a function of ka , where a is the radius of the resulting disk obtained by projecting the piston ($\eta_0 = 0.9848$) onto the xy plane for odd values of ℓ

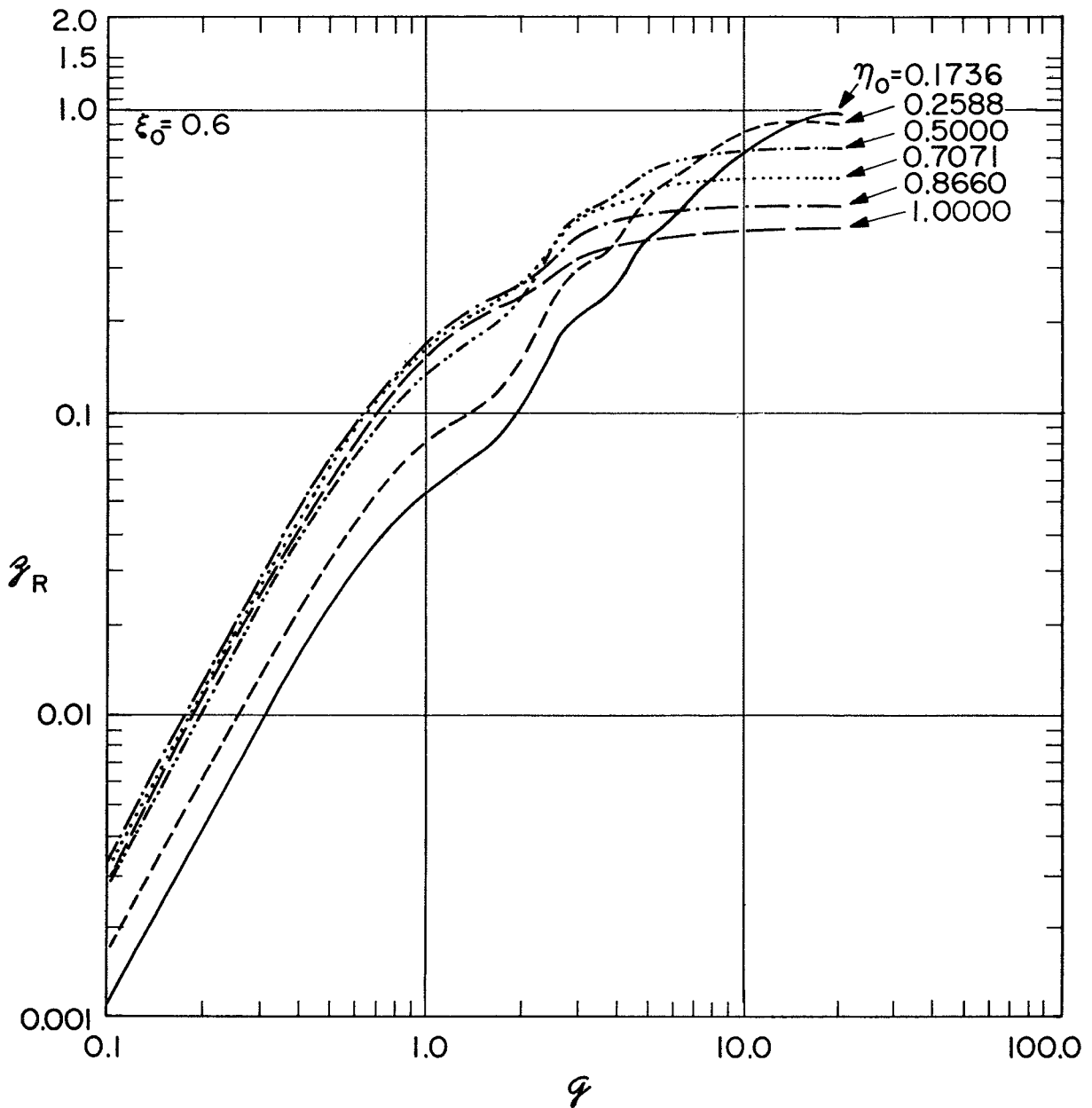


Fig. 21a - Radiation resistance density for rings on oblate spheroids as a function of $q = kd/2$ for the spheroid $\xi = 0.6$

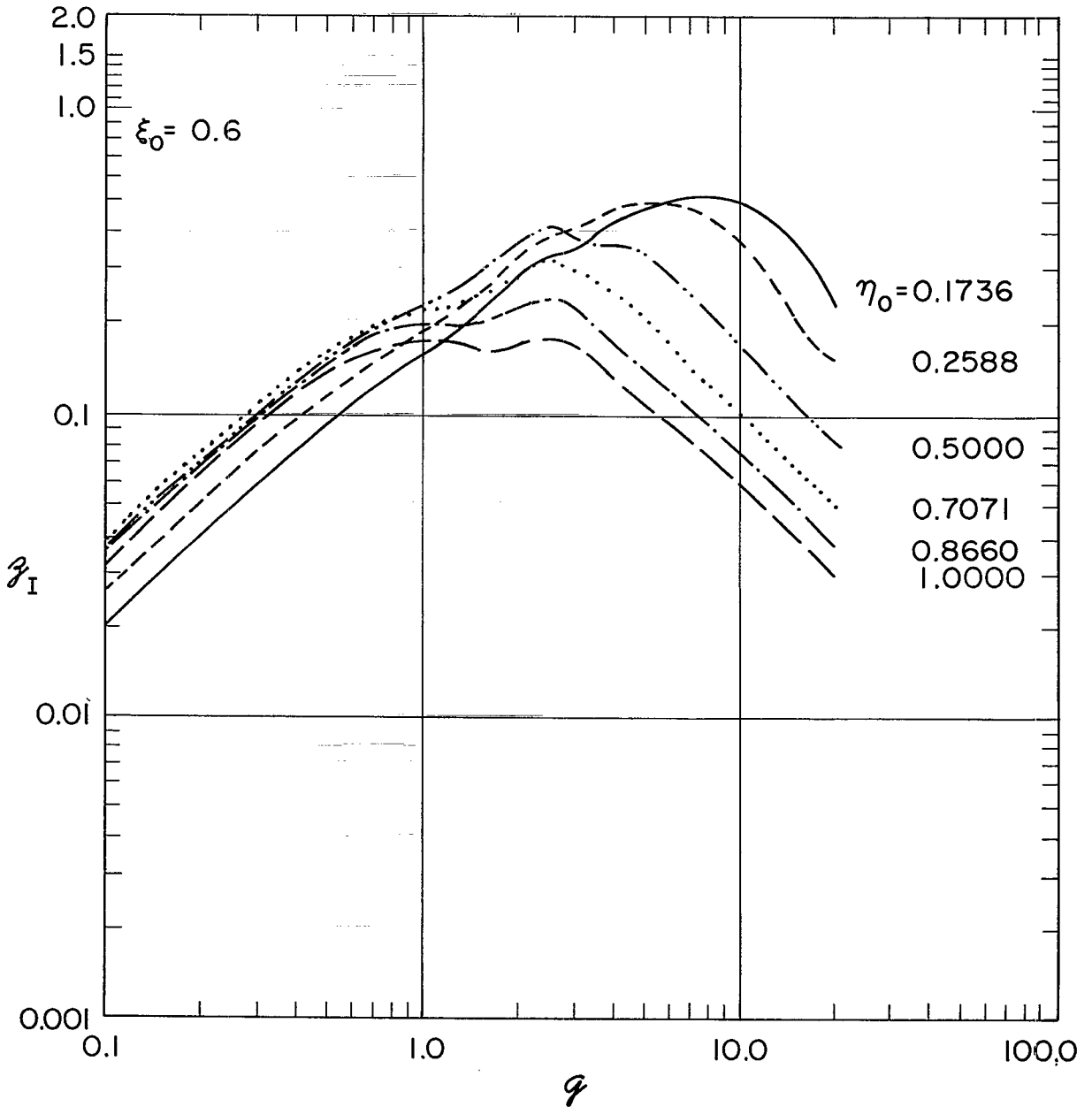


Fig. 21b - Radiation reactance density for rings on oblate spheroids as a function of $q = kd/2$ for the spheroid $\xi = 0.6$

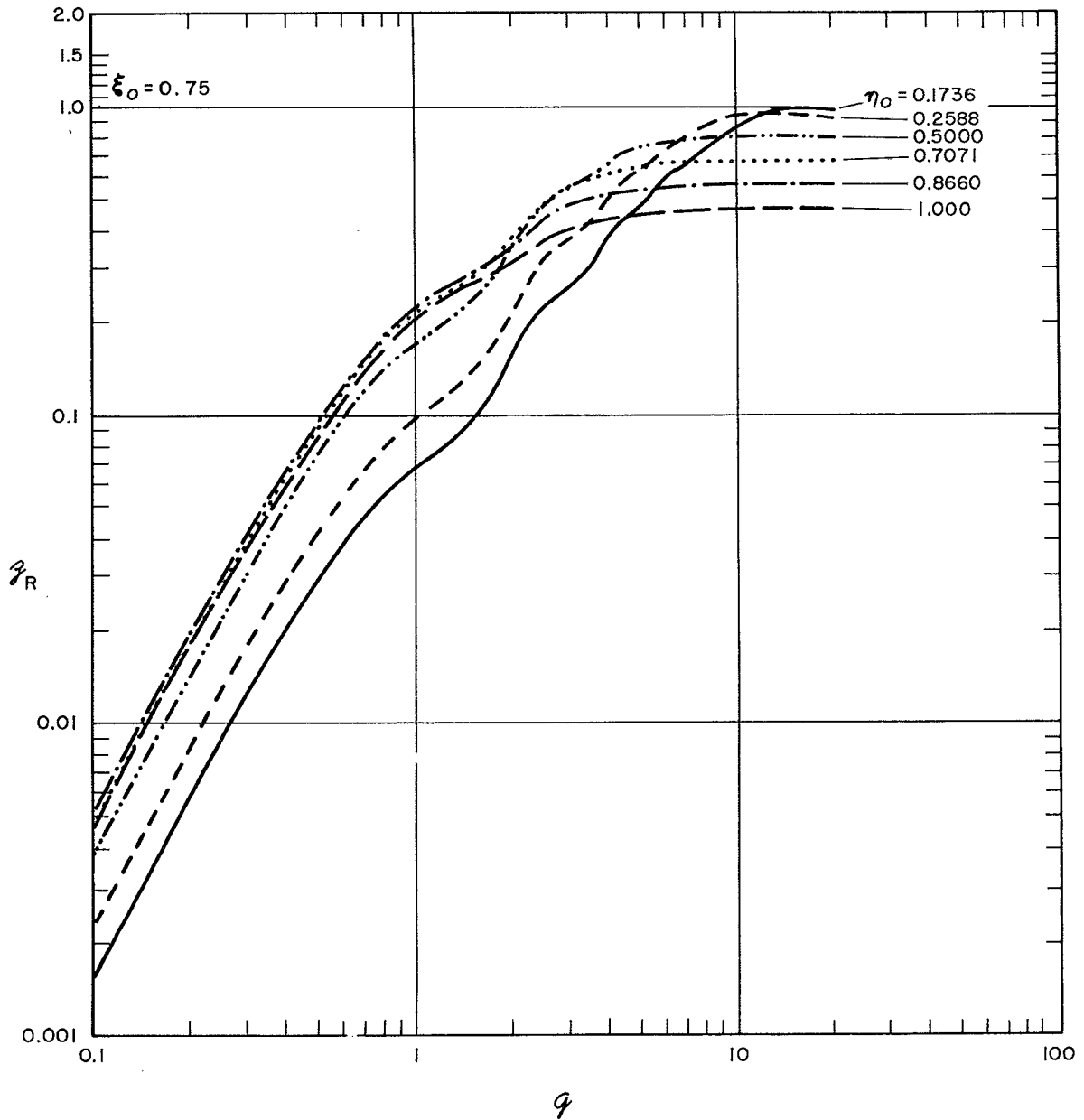


Fig. 22a - Radiation resistance density for rings on oblate spheroids as a function of $q = ka/2$ for the spheroid $\xi = 0.75$

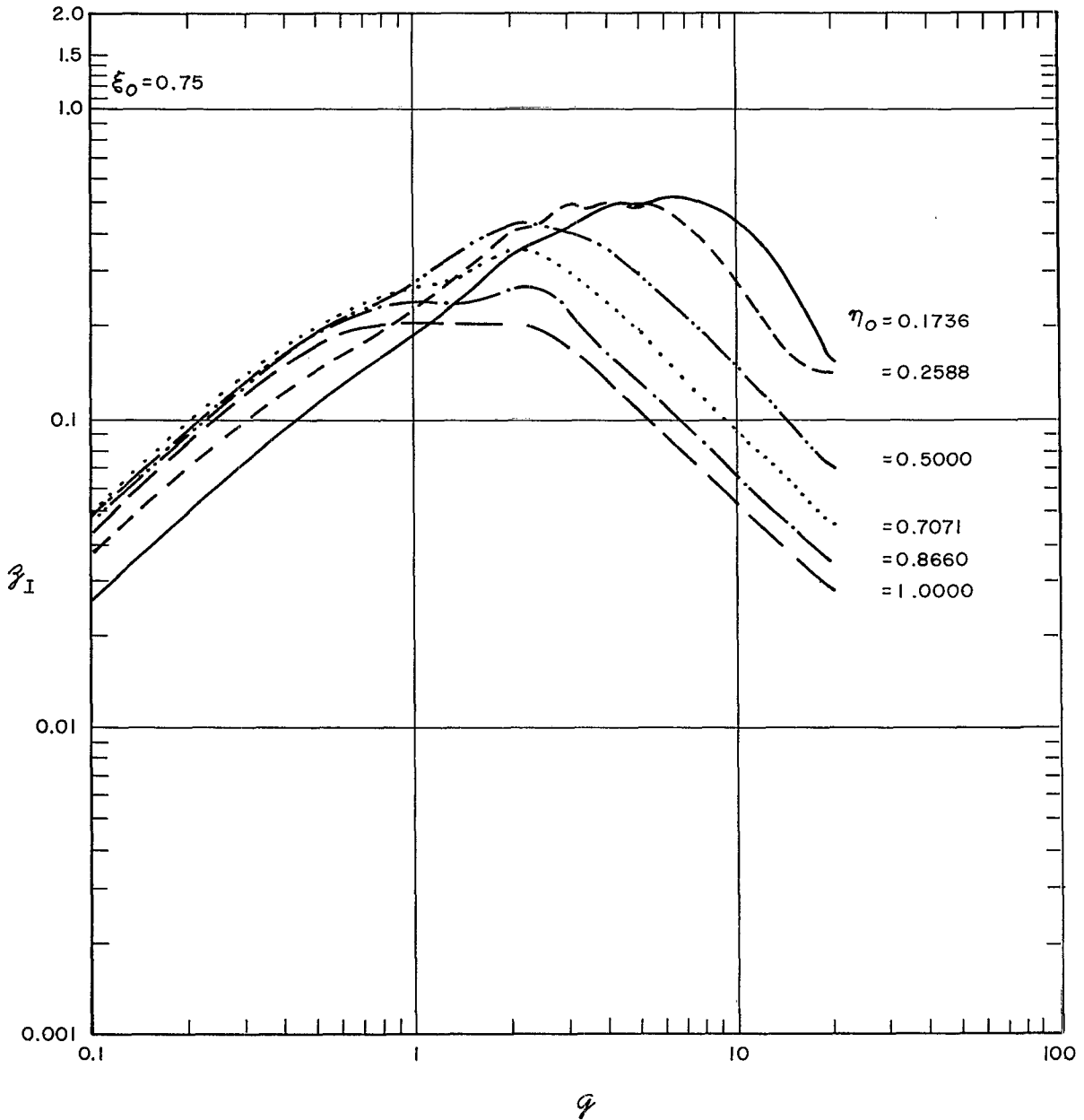


Fig. 22b - Radiation reactance density for rings on oblate spheroids as a function of $q = kd/2$ for the spheroid $\xi = 0.75$

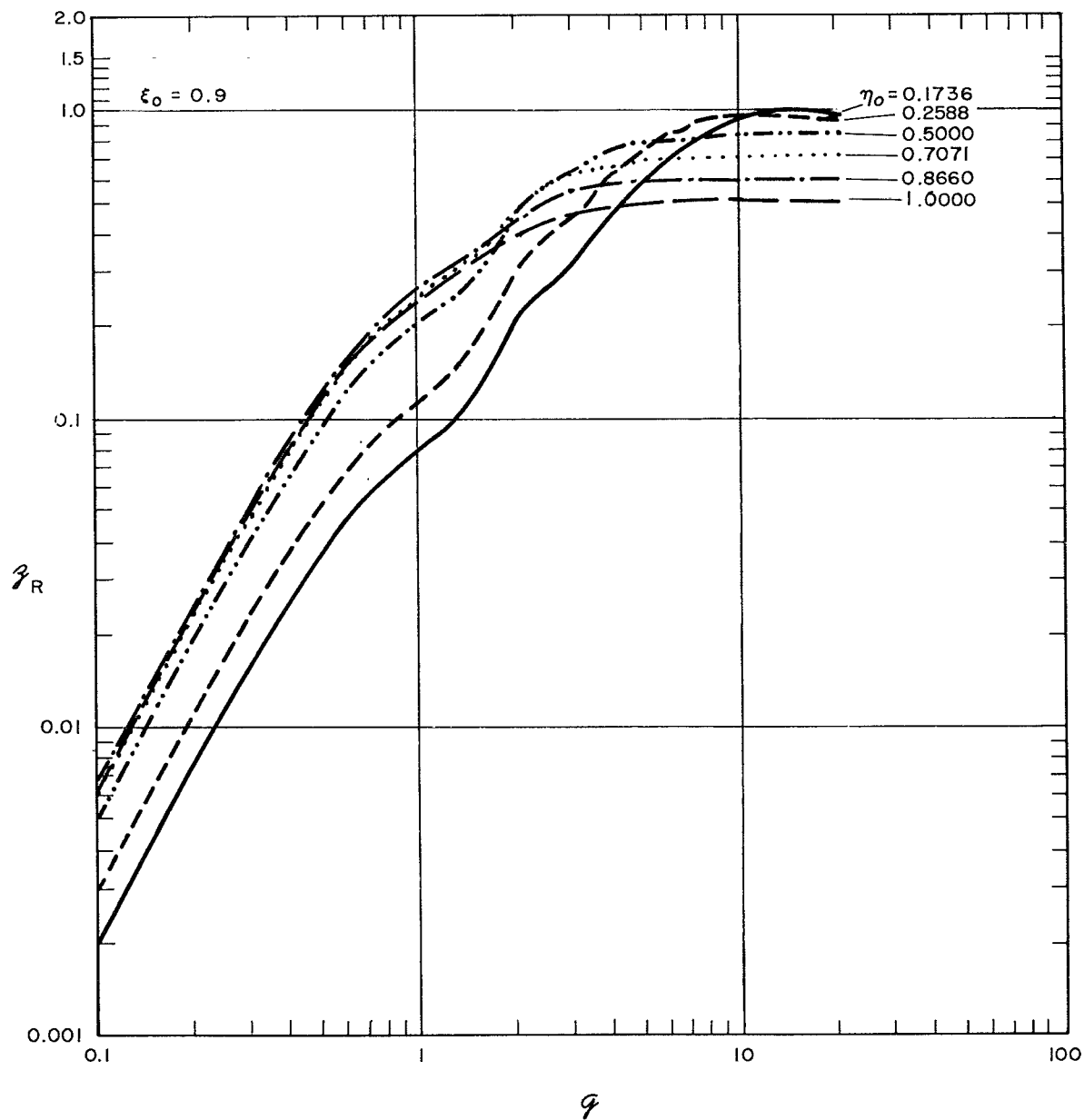


Fig. 23a - Radiation reactance density for rings on oblate spheroids as a function of $q = kd/2$ for the spheroid $\xi = 0.9$

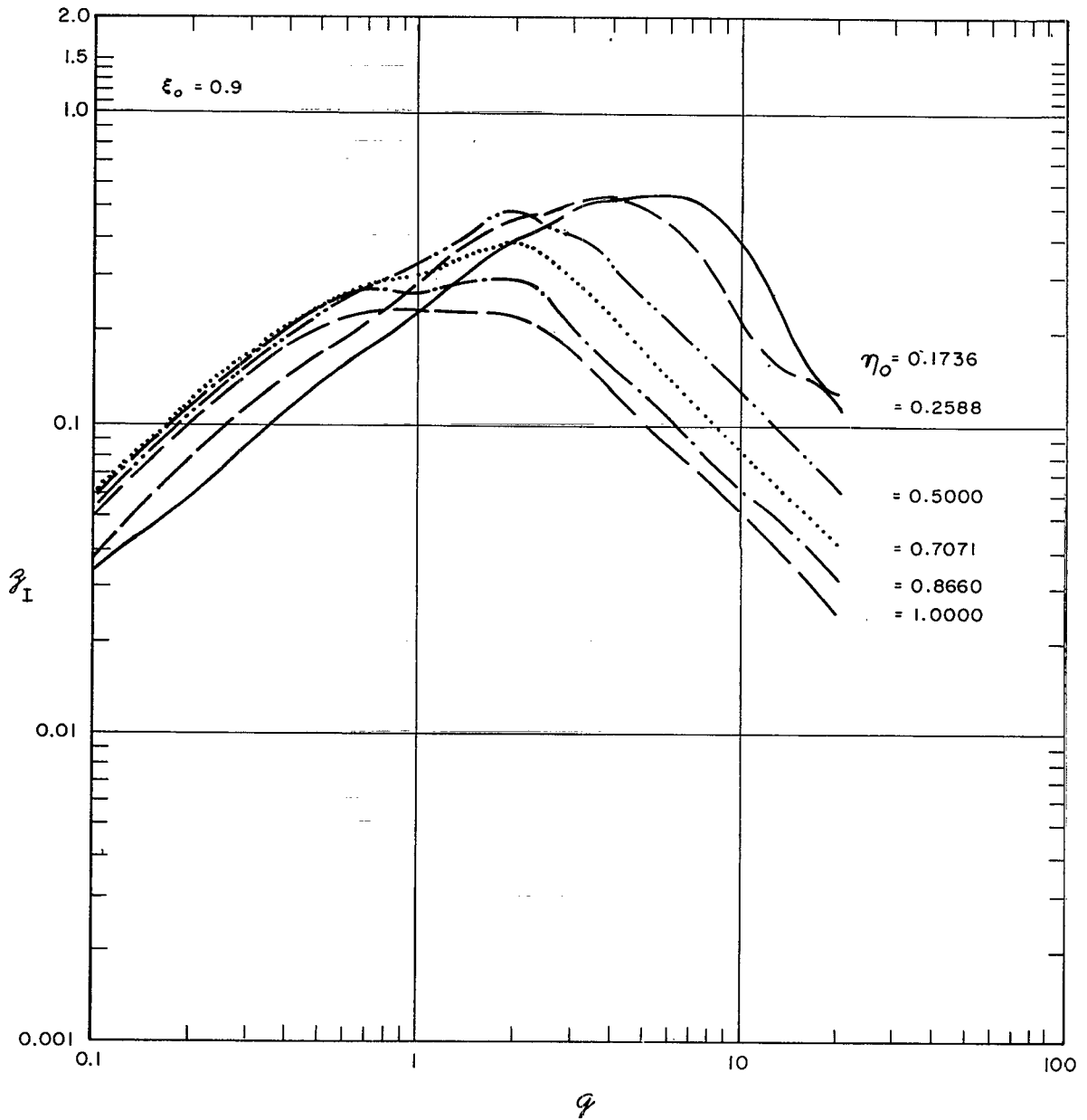


Fig. 23b - Radiation reactance density for rings on oblate spheroids as a function of $q = kd/2$ for the spheroid $\xi = 0.9$

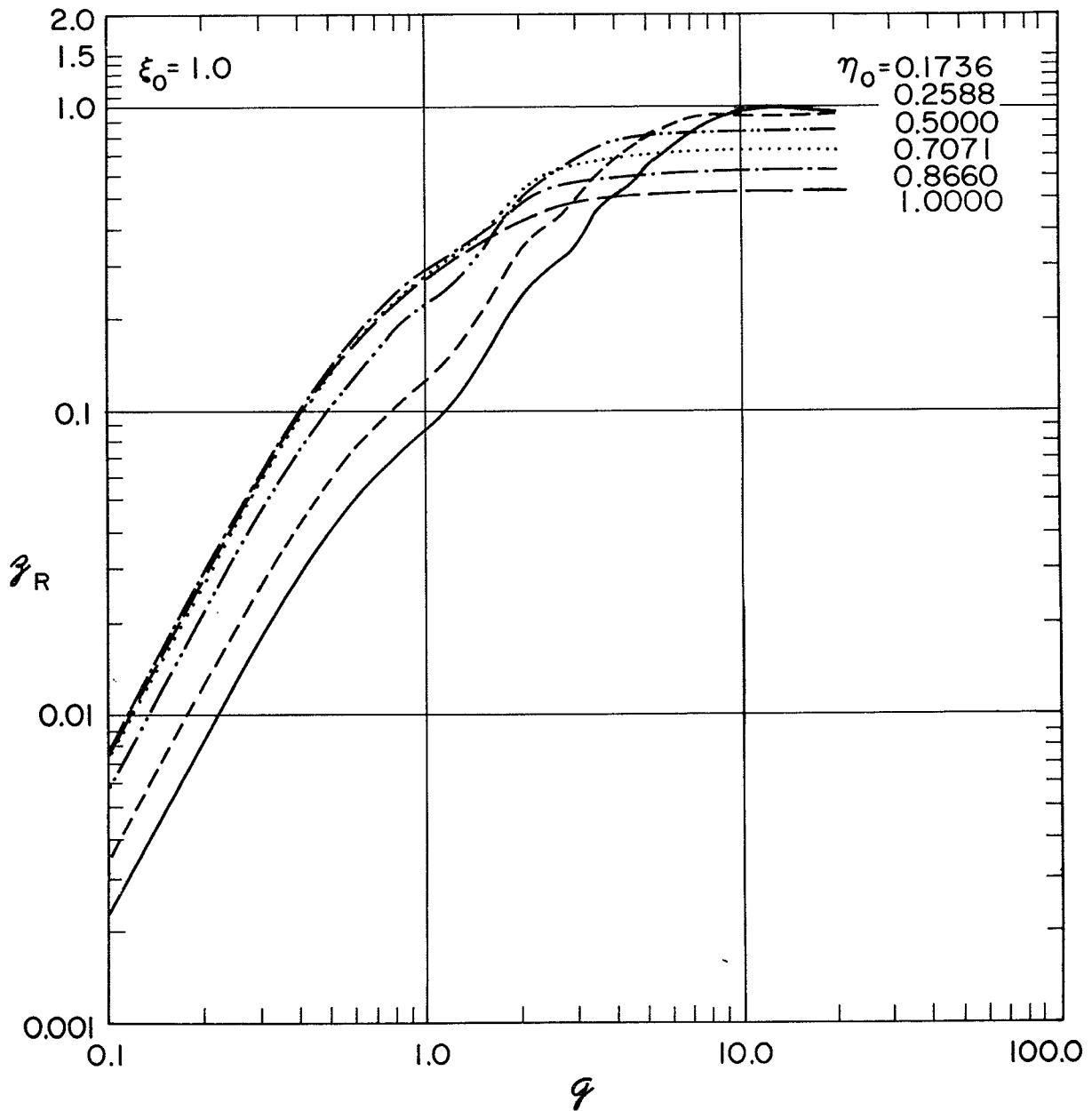


Fig. 24a - Radiation resistance density for rings on oblate spheroids as a function of $q = kd/2$ for the spheroid $\xi = 1.0$

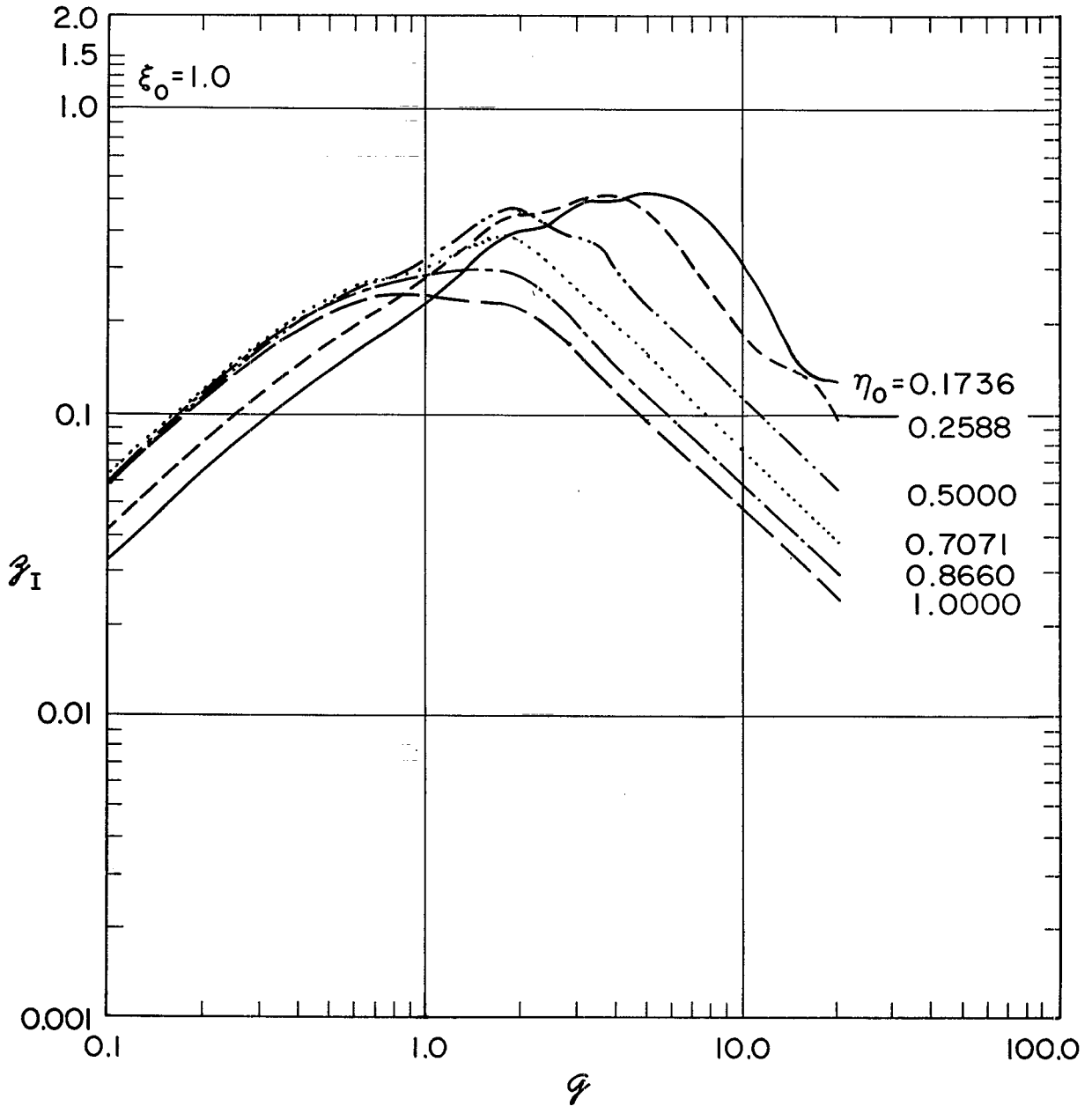


Fig. 24b - Radiation reactance density for rings on oblate spheroids as a function of $q = kd/2$ for the spheroid $\xi = 1.0$

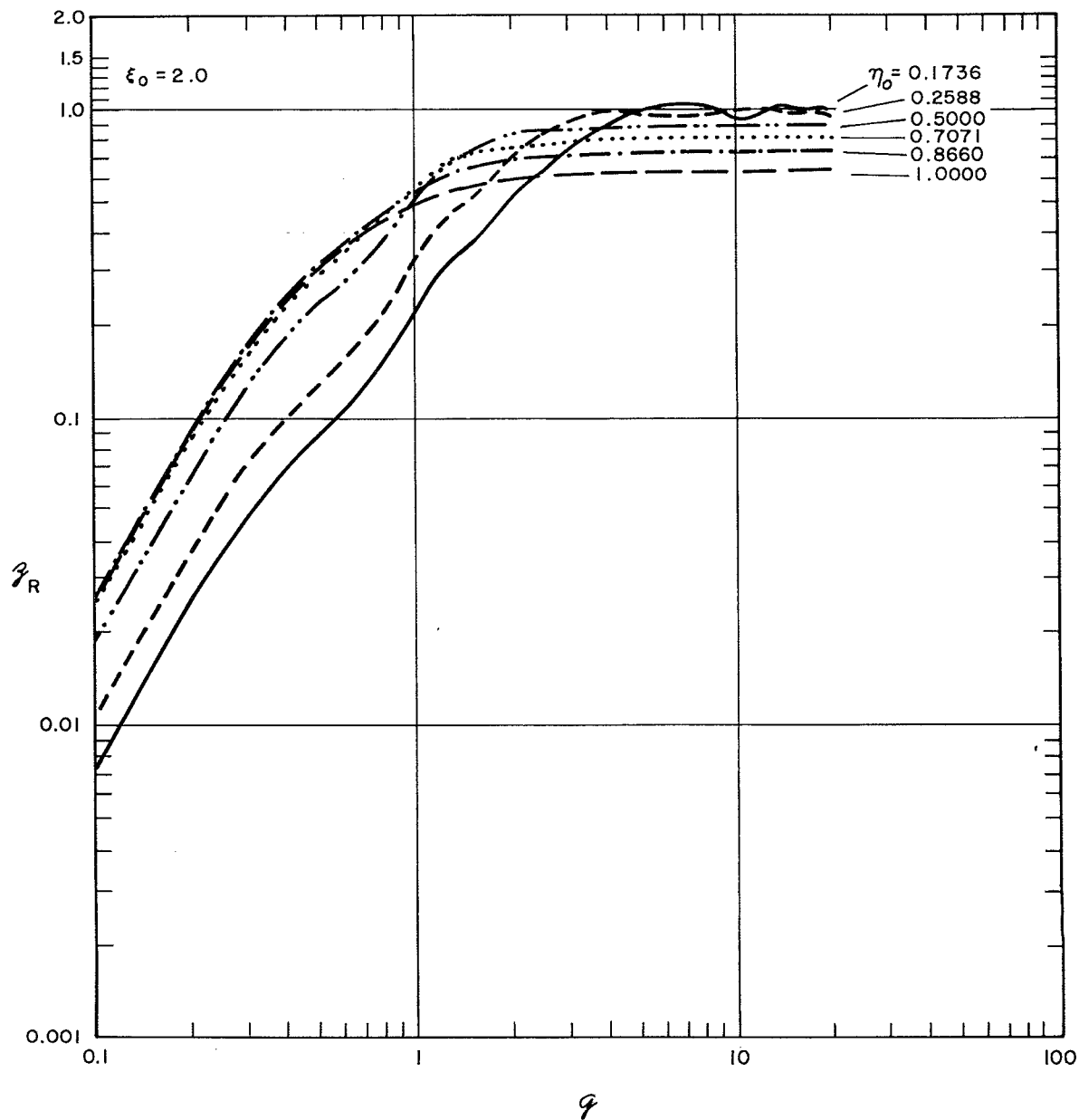


Fig. 25a - Radiation resistance density for rings on oblate spheroids as a function of $q = kd/2$ for the spheroid $\xi = 2.0$

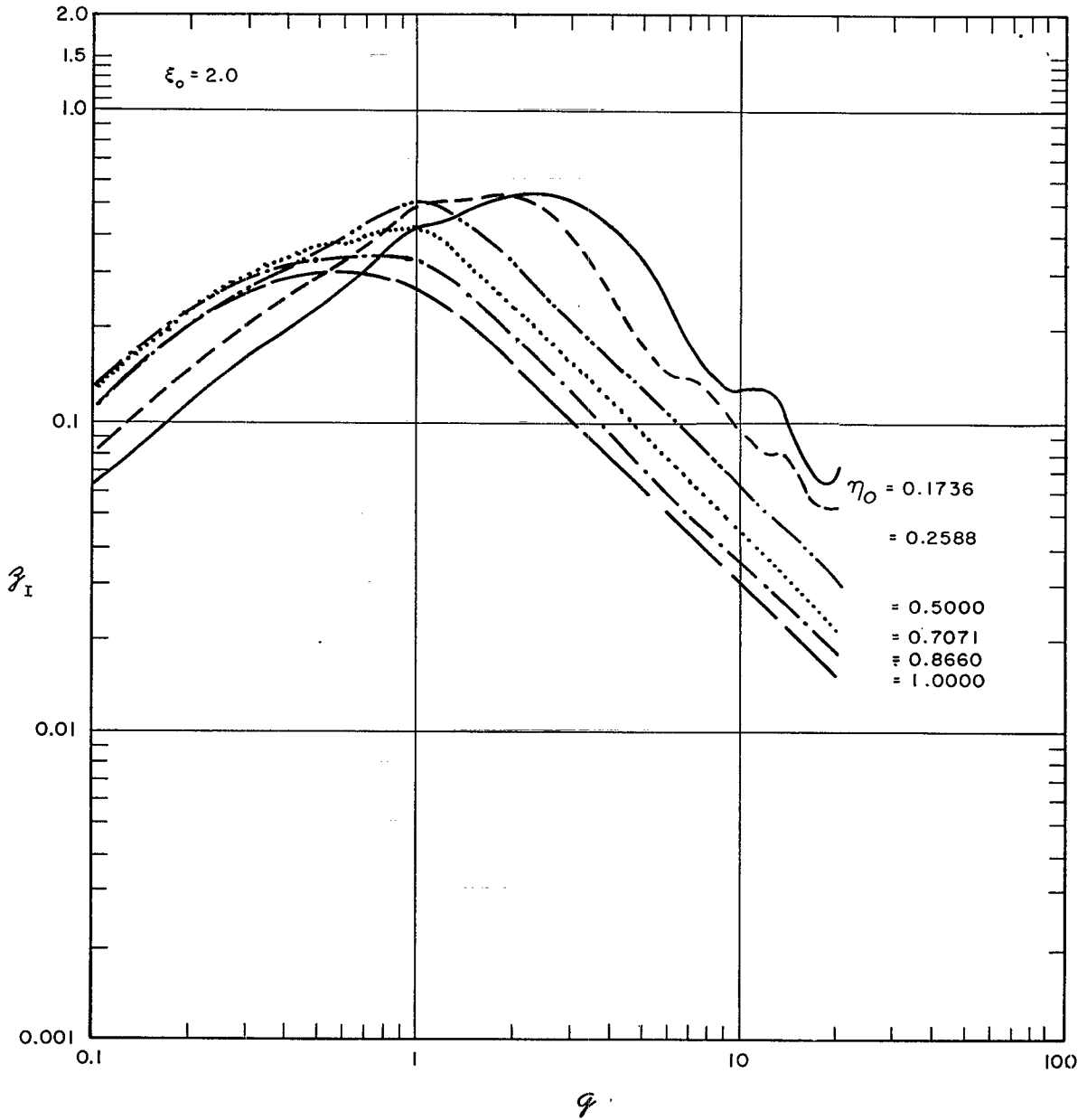


Fig. 25b - Radiation reactance density for rings on oblate spheroids as a function of $q = kd/2$ for the spheroid $\xi = 2.0$

REFERENCES

1. Flammer, C. , "Spheroidal Wave Functions," Stanford University Press, Stanford, Calif. 1957
2. Bouwkamp, C.J. , "Theoretische en Numerieke Behandeling van der Buiging door een Rone Opening," Diss. Groningen, Groningen-Batavia, 1941
3. Silbiger, A. , "Asymptotic Formulas and Computational Methods for Spheroidal Wave Functions," Cambridge Acoustical Associates, Inc. , Report U-123-48, Oct. 1961
4. Chertock, G. , "Sound Radiation From Prolate Spheroids," David Taylor Model Basin Report 1516, Nov. 1961
5. Nimura, T. , and Watanabe, Y. , "Sound Radiation from the Zonal Radiators," Tohoku University Science Report, Series B, 5:176 (1953)
6. Hanish, S. , "The Mechanical Self Resistance and the Mechanical Mutual Resistance of an Unbaffled Rigid Disk ($k < 1$) Radiating Sound from a Single Face into an Acoustic Medium," NRL Report 5538, Oct. 1960
7. Morse, P.M. , and Feshbach, H. , "Methods of Theoretical Physics," New York, McGraw-Hill, 1953
8. Hanish, S. , "The Mutual Mechanical Radiation Resistance for all Values of ka of an Unbaffled Circular Rigid Piston with Pressure Released Back," NRL Report 5513, Sept. 1960
9. Van Buren, A.L. , Baier, R.V. , and Hanish, S. , "A Fortran Computer Program for Calculating the Oblate Spheroidal Radial Functions of the First and Second Kind and Their First Derivatives," NRL Report 6959, 1970.
10. King, B.J. , and Van Buren, A.L. , "A Fortran Computer Program for Calculating the Prolate and Oblate Angle Functions of The First Kind and Their First and Second Derivatives," NRL Report 7161, July 1970.

DOCUMENT CONTROL DATA - R & D

(Security classification of title, body of abstract and indexing annotation must be entered when the overall report is classified)

1. ORIGINATING ACTIVITY (Corporate author) Naval Research Laboratory Washington, D. C. 20390		2a. REPORT SECURITY CLASSIFICATION Unclassified	
		2b. GROUP	
3. REPORT TITLE ACOUSTIC RADIATION IMPEDANCE OF CAPS AND RINGS ON OBLATE SPHEROIDAL BAFFLES			
4. DESCRIPTIVE NOTES (Type of report and inclusive dates) An interim report on one phase of a continuing NRL Problem			
5. AUTHOR(S) (First name, middle initial, last name) R. V. Baier			
6. REPORT DATE July 16, 1971		7a. TOTAL NO. OF PAGES 44	7b. NO. OF REFS 10
8a. CONTRACT OR GRANT NO. NRL Problem S01-29		9a. ORIGINATOR'S REPORT NUMBER(S) NRL Report 7207	
b. PROJECT NO. RR 102-08-41-5226		9b. OTHER REPORT NO(S) (Any other numbers that may be assigned this report)	
c.			
d.			
10. DISTRIBUTION STATEMENT Approved for public release; distribution unlimited			
11. SUPPLEMENTARY NOTES		12. SPONSORING MILITARY ACTIVITY Department of the Navy, Office of Navy Research Arlington, Virginia 22217	
13. ABSTRACT The acoustic radiation impedance seen by curved vibrating caps and rings located on hard baffles of oblate spheroidal shape has been analyzed using eigenfunction expansion in oblate spheroidal wave functions. With the help of extensive computer programs the formulas have been numerically evaluated. The results are presented in families of plotted curves showing the effect of curvature on the acoustic radiation impedance. Calculations were made for ranges in acoustic size of $0.1 \leq ka \leq 20$.			

14. KEY WORDS	LINK A		LINK B		LINK C	
	ROLE	WT	ROLE	WT	ROLE	WT
Underwater sound						
Underwater sound sources						
Sound transducers						
Sonar transducers						
Analysis (mathematics)						
Oblate spheroidal wave functions						
Impedance (mechanical)						
Acoustic fields						